Structural Characterization of β-Cardiac Myosin Subfragment 1 in Solution†

Katalin Ajtai, Susanna P. Garamszegi, Sungjo Park, Adolfo L. Velazquez Dones,‡ and Thomas P. Burghardt*

Department of Biochemistry and Molecular Biology, Mayo Foundation, 200 First Street SW, Rochester, Minnesota 55905

Received June 12, 2001; Revised Manuscript Received August 3, 2001

ABSTRACT: β-cardiac myosin subfragment 1 (βS1) tertiary structure and dynamics were characterized with proteolytic digestion, nucleotide analogue trapping kinetics, and intrinsic fluorescence changes accompanying nucleotide binding. Proteolysis of βS1 produces the 25, 50, and 20 kDa fragments and a new cut within the 50-kDa fragment at Arg369. F-actin inhibits cleavage of the 50-kDa fragment and fails to inhibit cleavage at the 50/20 kDa junction, suggesting βS1 presents an actoS1 conformation fundamentally different from skeletal S1. Time-dependent changes in Mg^{2+}-ATPase accompanying proteolysis identifies cleavage points that lie within the energy transduction pathway. The nucleotide analogue trapping kinetics reveal the presence of a reversible weakly actin attached state. Comparison of nucleotide analogue induced βS1 structures with the transient structures occurring during ATPase indicates analogue induced and transient structures are in a one-to-one correspondence. Tryptophan fluorescence enhancement accompanies the binding or trapping of nucleotide or nucleotide analogues. Isolation of Trp508 fluorescence shows it is an ATP-sensitive tryptophan and that its vicinity changes conformation sequentially with the transient intermediates accompanying ATPase. These studies elucidate energy transduction and suggest how mutations of βS1 implicated in disease might undermine function, stability, or efficiency.

Cardiac myosin, the motor protein functioning in the heart as the chemomechanical energy transducer (*2*), associates with actin to transduce chemical energy in ATP to mechanical work. The globular head portion of cardiac myosin, subfragment 1 (S1),[1,2] shares sequence (79% identity), the ATP hydrolysis scheme (*3*, *4*), the characteristics of an ATP sensitive tryptophan (*3*−*5*), a highly reactive thiol (*6*) and lysine residue (*7*), proteolytic digestion patterns (*8*), and other physical properties with skeletal myosin S1, suggesting their comparison in the investigation of the molecular mechanism of energy transduction (*9*). The skeletal and cardiac S1 analogy offers many points for comparison of which we involve two. First, we compared skeletal and cardiac S1 morphology and function with time-resolved limited proteolytic digestion and its correlation with changes in the ATP hydrolysis rate. We observed characteristic differences related to the exposure of surface loops to proteolysis, the participation of these surface loops in ATPase regulation, and the effect of actin binding on myosin structure. Second, starting from the available S1 crystal structures identifying regions for the structural characterization of cardiac S1 key to the transduction mechanism, we used substrate analogues and site-specific intrinsic or extrinsic optical probes to begin the structural characterization of these interesting regions. Each of these studies elucidating energy transduction are undertaken with the understanding that they also elucidate how the known mutations of cardiac S1 work to undermine function, stability, or efficiency.

The proteolytic digestion of S1 splits the protein into three fragments with molecular masses of 25, 50, and 20 kDa (*10*). The fragmentation pattern is characteristic to all of the myosins as the consequence of the domain organization of this protein with connecting surface loops accessible to proteolytic enzymes (*11*). The 25/50 junction, loop 1, and the 50/20 junction, loop 2, have important biochemical functions due to their proximity to the ATP binding site (loop 1) or to the actin binding region (loop 2) (*12*, *13*). Limited tryptic digestion of cardiac S1 generated similar fragments to that of skeletal S1 with slightly different molecular masses due to sequence differences in loops 1 and 2 (*13*); however, structural/functional differences between skeletal and cardiac S1 emerge. We found a new trypsin sensitive point in cardiac S1 within the 50-kDa fragment on a surface loop (cardiac-loop or C-loop, see Figure 1) at Arg369, dividing the fragment into two new peptides with molecular masses of about 20 and 30 kDa. The C-loop is located near to the actin binding site and its cleavage is inhibited by the presence of actin. Unlike skeletal S1 (*14*, *15*), actin binding does not inhibit the loop 2 cut. These data indicate interesting differences in the actomyosin interaction between skeletal and cardiac S1 that implicate new regions on S1 that are

† This work was supported by the National Institutes of Health Grant R01 AR39288 and the Mayo Foundation.

* Corresponding author: Phone 507 284 8120; Fax 507 284 9349; E-mail burghardt@mayo.edu.

‡ Present address: Department of Cellular and Molecular Medicine, School of Medicine, University of California at San Diego, La Jolla, CA 92093-0651.

[1] Abbreviations: 5′-iodoacetamidofluorescein (5′-IAF), aluminum fluoride complex (AlF_4^-), ATP sensitive tryptophan (AST), adenosine-5′-*O*-3-thiotriphosphate (ATPγS), beryllium fluoride complex (BeF_x), β-cardiac myosin subfragment 1 (βS1), circular dichroism (CD), hypertrophic cardiomyopathy (HCM), 4-(2-hydroxyethyl)-1-piperazine ethane sulfonic acid (HEPES), phosphate analogue (PA), inorganic phosphate (P_i), reactive lysine residue or Lys83 (RLR), myosin subfragment 1 (S1), most reactive thiol or Cys705 (SH1), 2,4,6-trinitrobenzene sulfonate (TNBS), trinitrophenyl- (TNP-), ultraviolet (UV), vanadate (Vi).

[2] Myosin sequence numbering is from human β cardiac (*1*).

10.1021/bi0112098 CCC: $20.00
Published on Web 09/14/2001

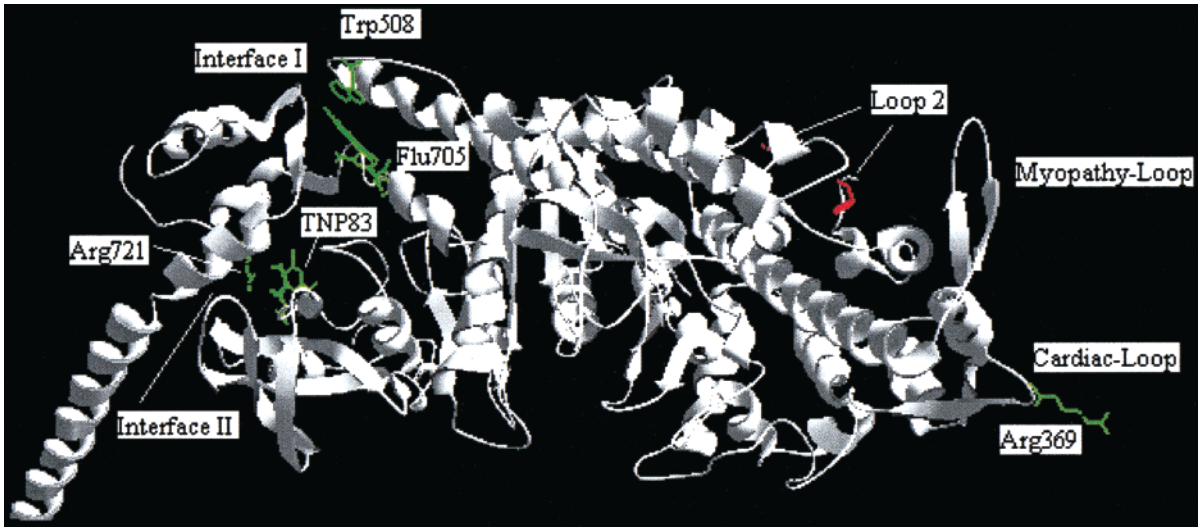

FIGURE 1: The ribbon diagram and selected side chains of modified skeletal S1 representing β-cardiac S1. The cardiac-loop and Arg369 identify a trypsin cutting point in βS1. The myopathy-loop identifies a site where the most common mutations in HCM occur (*32*, *90*). Loop 2, missing from the crystal structure, connects the red residues shown. Residues connected by loop 1 are not visible in this view of S1 but lie near to the catalytic site. Interface I contains the ATP sensitive tryptophan (Trp508) and 5′-IAF modifying the reactive thiol (Flu705). Interface II contains the reactive lysine residue modified with TNP (TNP83) and Arg721.

involved with actin. Furthermore, cuts at loop 1 and the C-loop dramatically alter ATPase activity in cardiac S1, directly implicating them in energy transduction pathways.

Myosin S1 crystal structures, including skeletal, promote the idea that the molecule may be viewed in three parts that catalyze ATP and bind actin (catalytic), conduct energy transduction (converter), and transport the load (lever arm) (*16*−*18*). These same structures suggest the catalytic and lever arm domains remain structurally intact but change their relationship, while the converter domain changes conformation during energy transduction. This view of transduction calls attention to the domain interfaces where conformation change and work production are highly correlated. It is within these interfaces that several mutations implicated in familial hypertrophic cardiomyopathy (HCM) affect myosin function (*9*, *19*−*21*) and where we focus efforts to structurally characterize cardiac S1. The interfaces I or II in Figure 1, contain the reactive thiol (SH1 or Cys705) and ATP sensitive tryptophan (Trp508) (*22*−*28*) or the reactive lysine residue (RLR or Lys83) (*29*, *30*).

Facilitating the structural characterization of energy transduction are the nucleotide analogues that occupy the active site of S1 and constrain the protein to indefinitely assume conformations mimicking those of the transient intermediates in the ATPase cycle. The analogues were shown to work in this capacity for skeletal, smooth, and dictyostelium S1 by a variety of criteria including crystallographic structure determination (*17*, *31*, *32*) and spectroscopic signature characterization (*33*, *34*). Previously, their effect on cardiac S1 was limited to a single analogue that was shown to work analogously to that in skeletal S1 (*35*). Herein, we study several of the nucleotide analogues and characterize their effect on cardiac S1 by comparing the analogue induced with the real intermediate structures present during steady-state ATPase. We also investigate substrate trapping kinetics as a means to characterize cardiac S1 and compare its behavior with that of skeletal S1. Skeletal and cardiac S1 trapping kinetics exposed the presence of a long-lived nucleotide analogue-bound actoS1 intermediate, analogous to the weakly bound myosin cross-bridge in skeletal muscle fibers (*36*).

MATERIALS AND METHODS

Chemicals. ATP, ADP, sodium azide, $BeCl_2$ (dissolved in 1% HCl), dimethylformamide (DMF), dithiothreitol (DTT), HEPES, phenylmethylsulfonyl fluoride (PMSF), carbonic anhydrase II (human erythrocyte), and Tris base are from Sigma (St. Louis, MO). Acrylamide (ultrapure) is from ICN (Aurora, OH). Proteolytic enzymes TPCK-trypsin and TLCK α-chymotrypsin are from Worthington Biochemical (Freehold, NJ). TNBS (2,4,6-trinitrobenzenesulfonic acid) is from Fluka (Milwaukee, WI), 5′-iodoacetamidofluorescein (5′-IAF) from Molecular Probes (Eugene, OR), and ATPγS from Roche Molecular Biochemicals (Indianapolis, IN). The ADP contamination of ATPγS is less than 5% according to polyethyleneimine cellulose thin-layer chromatography (*37*). All other chemicals are reagent grade. KF stock solutions were prepared on the day of the experiment. Bovine α-thrombin β-chain is a generous gift of Dr. W. G. Owen of Mayo Clinic.

Preparation of Proteins. Rabbit skeletal myosin was prepared from back and leg muscles by the method of Tonomura et al. (*38*). S1 was obtained by digestion of myosin filaments with α-chymotrypsin as described by Weeds and Taylor (*39*). The skeletal S1 used in our experiments contains a mixture of isoenzymes. Sodium dodecyl polyacrylamide−gel electrophoresis (SDS−PAGE) of proteins or their fragments was carried out according to Laemmli (*40*) in 7, 12, or 15% acrylamide gels.

β-Cardiac myosin was prepared from bovine heart ventriculum by combination of the protocols of Tada et al. (*41*) and Muhlrad et al. (*7*) with several modifications. Myosin was extracted from minced, washed ventriculum for 10 min at 4 °C with "Guba-Straub" solution containing 0.3 M KCl, 1 mM $MgCl_2$, 10 mM sodium pyrophosphate, 1 mM DTT, and 0.15 M potassium phosphate buffer, pH 6.5. After the solubilized myosin was separated from the tissue by cen-

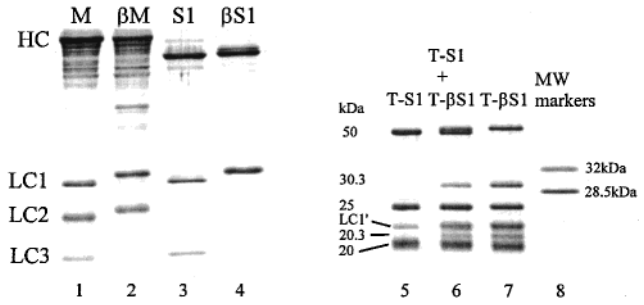

FIGURE 2: Coomassie stained SDS−PAGE from rabbit skeletal and cardiac myosin. Lanes 1−4 are skeletal myosin (M), cardiac myosin (βM), purified chymotryptic S1, and βS1. Lanes 5 and 7 are the tryptic fragments of S1 (T-S1) and βS1 (T-βS1). Lane 6 contains both T-S1 and T-βS1. Lane 8 has thrombin (32 kDa) and carbonic anhydrase (28.5 kDa) molecular weight (MW) markers. The T-S1 and T-βS1 samples shown were digested for 30 min with a 1:50 w/w ratio of trypsin:S1. Samples contain the myosin heavy chain (HC), light chains (LC) 1−3, and digestion fragments with weights given in kilodaltons (kDa). LC1′ is the digestion product of LC1.

trifugation, three cycles of precipitation by dilution and solubilization eliminated contaminating soluble proteins. A high salt-pyrophosphate wash (0.6 M KCl, 10 mM sodium pyrophosphate, 1 mM DTT, 1 mM $MgCl_2$, 0.2 mM PMSF in 50 mM Tris-HCl, pH 8.0) followed by ultracentrifugation (2 h 250000*g*) removed actin. β-Cardiac myosin was stored in 50% glycerol solution for months without any loss of enzymic activity or proteolytic degradation. β-Cardiac myosin subfragment 1 (βS1) was prepared by digesting β-cardiac myosin filaments for 10 min at 25 °C with α-chymotrypsin in a ratio of 1:300 in 0.1 M NaCl, 1 mM EDTA, 10 mM sodium phosphate buffer, pH 7.0. Addition of 0.2 mM PMSF stops the digestion, and the βS1 was separated by ultracentrifugation. Further purification was performed by using DEAE Sepharose Fast Flow ionic exchange chromatography (Amersham Pharmacia Biotech., Uppsala, Sweden). The final product is 99% βS1 (by weight) with high K^+EDTA-ATPase activity. The SDS−PAGE of cardiac and rabbit skeletal myosin and purified chymotryptic βS1 are shown in Figure 2. Rabbit skeletal myosin (M) has three light chains (LC1, LC2, and LC3), while LC3 is missing in the cardiac myosin (βM). βS1 has only LC1 while S1 contains both LC1 and LC3.

G-actin was prepared by a standard protocol from rabbit skeletal muscle acetone powder according to Pardee and Spudich (*42*).

Protein concentrations were obtained with absorbance using an A(1%) at 280 nm of 5.7 for skeletal and 5.33 for cardiac myosin, 7.45 for S1 and βS1, and A(1%) at 290 nm of 6.4 for actin. Molecular masses were assumed to be 500, 115, and 42 kDa for myosin, S1, and actin.

ATPase Assay. The ATPase activity of skeletal or cardiac S1 was measured from organic phosphate production using the Fiske and Subbarow method (*43*), and expressed as percent of control S1. K^+EDTA-ATPase measurements were made on samples at 25 °C from 1-mL aliquots containing 20−40 μg of S1, 2 mM ATP, 0.6 M KCl, 6 mM EDTA, and 25 mM Tris-HCl at pH 8.0. Ca^{2+}-ATPase was measured as for K^+EDTA-ATPase, except 6 mM $CaCl_2$ replaced EDTA. When estimating the inhibition of the ATPase due to trap formation in chemically modified S1, Ca^{2+}-ATPase was measured with 20 mM $CaCl_2$ to avoid competition from Mg. Mg^{2+}-ATPase measurements were made on samples at 25 °C from 1-mL aliquots containing 680 μg S1, 4 mM ATP, 30 mM KCl, 4 mM $MgCl_2$, and 25 mM Tris-HCl, pH 8.0, and without a deproteinization-step as suggested by Tashima (*44*).

Control ATPase activity values are given for S1 or βS1 in units of μmol of P_i (mg of S1)$^{-1}$ min^{-1}. K^+EDTA-ATPase activities are 9.5 ± 1.0 or 2.7 ± 0.27, Ca^{2+}-ATPase activities are 1.2 ± 0.1 or 0.35 ± 0.06, and Mg^{2+}-ATPase activities are 0.027 ± 0.005 or 0.0065 ± 0.0001.

Chemical Modification of Proteins. Skeletal or cardiac S1 was trinitrophenylated according to published protocols (*7*, *45*). A 2.2-fold molar excess of TNBS was added to 60−80 μM S1 in 30 mM KCl and 0.2 mM PMSF, 100 mM Tris-HCl buffer, pH 7.8. βS1 was trinitrophenylated in the same condition except the KCl concentration was 0.5 M. After incubation at 25 °C for 10 min, the reaction was terminated by addition of 2 mM DTT. Excess TNBS was removed by dialyzing twice against 100 volumes of 1 mM DTT, 60 mM KCl, 0.1 mM PMSF, and 30 mM HEPES, pH 7.0, at 4 °C (w/o DTT in the second dialysis). The number of TNP groups introduced was obtained from absorbance at 345 nm using ϵ_{345} = 14500 (Mcm)$^{-1}$ according to Okuyama and Satake (*46*). For calculation of the concentration of TNP-modified S1 or βS1 (TNP-S1 or TNP-βS1), the absorbance at 280 nm was corrected according to the formula: corrected (A_{280}) = observed (A_{280}) − 0.362 × observed (A_{345}). TNP-S1 or TNP-βS1 contains 0.8−1.1 TNP/S1.

Labeling specificity was also investigated with Mg^{2+}, Ca^{2+}, and K^+EDTA-ATPase activities. The effect of modification of Lys83 on the ATPase activities is expressed as the % of the unmodified control ATPase activity for S1 or βS1. K^+-EDTA-ATPases are 17 or 26% of control, Ca^{2+}-ATPases are 110 or 95%, and Mg^{2+}-ATPases are 800 or 426%. The changes in the different ATPase activities upon TNP modification of S1 or βS1 shows 70−80% of the label resides on Lys83 as shown previously (*7*, *47*).

The reactive thiol of skeletal or cardiac S1 was modified with 5′-IAF according to published protocols (*6*, *48*). S1 was modified with 2-fold and βS1 with 2−2.5-fold molar excess of 5′-IAF for 12 h at 4 °C in 60 mM KCl, 0.1 mM PMSF, and 30 mM HEPES, pH 7.0. Excess dye was removed by gel filtration on a PD10 column (Amersham). This procedure produced fluorescein-labeled S1 or βS1 with 70−80% of the SH1's modified and no detectable nonspecific label (*48*). Figure 3 shows the fluorescence image of the SDS−PAGE of the intact and the tryptic digest of fluorescein labeled βS1. Fluorescein fluorescence is located only on the βS1 heavy chain or its 20-kDa proteolytic fragment containing SH1 (lanes 8 and 9).

Labeling specificity was also investigated with Ca^{2+} and K^+EDTA-ATPase activities. The effect of modification of SH1 on the ATPase activities is expressed as the % of the unmodified control ATPase activity for S1 or βS1. Proteins containing 0.7−0.8 5′-IAF/S1 had K^+EDTA-ATPase activities of 22 or 31% of control and Ca^{2+}-ATPase activities of 424 or 330%. The changes in the different ATPase activities upon fluorescein modification of S1 or βS1 shows 70−80% of the label resides on SH1 as shown previously (*6*, *48*).

Time-Resolved Proteolysis. Skeletal or cardiac S1 was digested with trypsin according to Bálint et al. (*49*) and Muhlrad et al. (*50*). For the tryptic digestion, the reaction

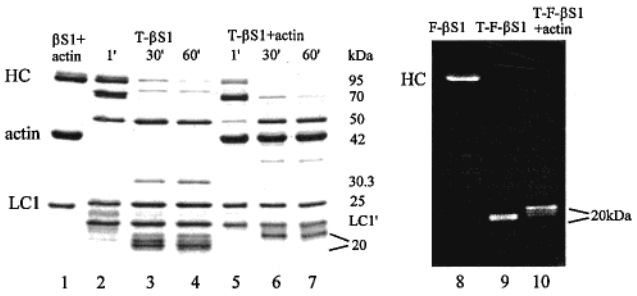

FIGURE 3: Coomassie stained and fluorescent SDS−PAGE from unlabeled and 5′-IAF labeled βS1 digested with trypsin in the absence and presence of actin. Abbreviations are as in Figure 2. Lane 1 contains actoβS1. Lanes 2−4 βS1 and lanes 5−7 actoβS1 digested with trypsin and samples taken at 1, 30, and 60 min. Lane 8 contains 5′-IAF labeled βS1 (F-βS1). Lane 9 shows the fluorescent 20-kDa fragment of T-F-βS1. Lane 10 shows the fluorescent 20-kDa fragment of actoF-βS1 digested with trypsin. The digestion was performed in a molar ratio of 1:3 for βS1:actin and w/w ratio of 1:50 for trypsin:βS1.

mixture included 60 mM KCl (no KCl for skeletal S1) and 50 mM Tris-HCl, pH 8.0, with a final S1 concentration of 2 mg/mL. All reactions were carried out at 25 °C. Digestion was started with the addition of trypsin. The weight ratios of trypsin to S1 varied as 1:50, 1:100, or 1:200 depending on the experiment. In experiments when the effect of actin was tested the S1:actin molar ratio was 1:3. The proteolysis reaction was investigated in time by removing aliquots from the digestion mixture at intervals following trypsin addition. The digestion was stopped either by adding soybean trypsin inhibitor in a w/w ratio of trypsin to inhibitor of 1:2 or by boiling the aliquot with an equal volume of sample buffer. Gel scanning, the quantitative analysis of the digestion products, and the interpretation of these data in terms of the kinetics of proteolysis is described in the appendix.

Protein Sequencing. The peptide bands from SDS−PAGE gels were electroblotted to poly(vinylidene difluoride) (PVDF) and analyzed by Edman degradation microsequencing using the Applied Biosystems 492 Procise Protein sequencing system (Applied Biosystems, Foster City, CA) with pulsed liquid chemistry. The data were collected and analyzed using the Applied Biosystems model 610 sequencing software. All microsequencing was done by the Mayo Protein Core Facility.

Formation of Trapped Complexes. Native and modified S1 and βS1 (17−30 μM) were incubated in 60 mM KCl, 1 mM $MgCl_2$, 0.2 mM ADP (5 mM KF for Be and Al) and 30 mM HEPES, pH 7.0, at 25 °C for 5 min. Then $BeCl_2$ (0.2 mM), Vi (0.2 mM), or $AlCl_3$ (0.4 mM for βS1, 1 mM for F-S1 or F-βS1) was added, and the incubation was continued at 25 °C for 25 min. Stable trapped complex formation was checked by measuring K^+EDTA-ATPase activity. In the case of SH1 or RLR modified S1, active site trapping was followed by measuring Ca^{2+}-ATPase. Under these conditions, ATPase inhibition was >90%.

Trap formation kinetics was investigated by the same procedure except that ATPase inhibition was observed as a function of time and concentration of phosphate analogue. Aliquots from the reaction mixture were removed at several time intervals following addition of the phosphate analogue. The dilution of the aliquot in the ATPase assay buffer stopped the reaction.

Trap Stability. The trapped nucleotide analogue (S1·MgADP·PA) spontaneous or actin-induced dissociation kinetics were studied following the removal of the excess reagents by gel filtration in a buffer containing 30 mM HEPES, 60 mM KCl, 1 mM $MgCl_2$, 0.2 mM DTT, 0.1 mM PMSF, pH 7.0. Spontaneous complex dissociation was followed by incubating the S1·MgADP·PA at 20 °C and observing the recovery of ATPase (K^+EDTA- or Ca^{2+}-) activity by time. Actin-induced complex dissociation was observed according to Werber et al. (*51*), in which trapped S1 (5 μM) was incubated with 10 μM F-actin at 20 °C in 50 mM KCl, 1 mM $MgCl_2$, and 30 mM Tris-HCl pH 8.0. The K^+EDTA-ATPase recovery was measured at intervals following the addition of actin by taking aliquots from the incubation mixture.

Fluorescence Intensity and Quenching. Tryptophan fluorescence intensities were measured at 20 °C on a SLM 8000 (SLM Instruments, Urbana, IL) with monochromator bandwidths of 1−2 nm. Tryptophans in cardiac or skeletal S1 were excited at 298 nm and emission intensity estimated by integrating over the band from 315 to 360 nm. All measurements were made on 1.2 μM protein in 1 mM $MgCl_2$, 60 mM KCl, and 25 mM HEPES, pH 7.0. We observed the total tryptophan fluorescence intensity changes upon binding of nucleotide, or the trapping of a nucleotide analogue, by native S1 or βS1. We also isolated emission from the ATP sensitive tryptophan (AST) by differential spectroscopy and observed AST fluorescence enhancement and acrylamide quenching.

Differential spectroscopy isolates AST emission by forming an intensity difference, ΔI, between perturbed and unperturbed systems. The perturbation alters AST emission such that

$$\Delta I = I(\mathrm{P}) - I(\mathrm{U}) \qquad (1)$$

where P and U signify perturbed and unperturbed systems, removes contributions from all tryptophans other than the AST (*23*). The choice of perturbant determines whether emission is (i) solely from the unperturbed AST, or (ii) a weighted difference from perturbed and unperturbed AST. AST emission is known to be totally quenched by the modification of SH1 with fluorescein in skeletal S1, while emission from other tryptophans in the protein is unaffected (*52*, *53*). Formation of ΔI with fluorescein modifying SH1 in the perturbed protein (method 1) isolates emission solely from the unperturbed AST. Bound nucleotides or trapped nucleotide analogues perturb AST emission by altering skeletal S1 conformation at Trp508 where the catalytic, converter, and lever arm domains interface (Figure 1) (*29*, *30*). Formation of ΔI with bound nucleotides or trapped nucleotide analogues acting as perturbant (method 2) isolates heterogeneous AST emission originating from both the perturbed and unperturbed AST.

The total quenching of the AST with fluorescein (method 1), verified experimentally for skeletal S1 (*23*), is likely to carry over to cardiac S1 because of sequence homology (79% identity between human βS1 and chicken skeletal S1 using BLASTP vs 2.1.2) and their similar responses to fluorescein labeling where identical quenching of ∼1/5 of the total tryptophan fluorescence is observed. Results derived from nucleotide perturbants (method 2) are valid for an AST in

Scheme 1

$$\begin{array}{ccccccc} M + ATP & \leftrightarrow & M^*.ATP & \leftrightarrow & M^{**}.ADP.P_i & \leftrightarrow M^{\wedge}.ADP + P_i & \leftrightarrow M + ADP \\ \updownarrow & & \updownarrow & & \updownarrow & \updownarrow & \updownarrow \\ A.M + ATP & \leftrightarrow & A\cdots M^*.ATP & \leftrightarrow & A\cdots M^{**}.ADP.P_i & \leftrightarrow A.M^{\wedge}.ADP + P_i & \leftrightarrow A.M + ADP \end{array}$$

↖Force Production

any protein, but the assignment of the AST to Trp508 could be sequence dependent. Trp508 has been shown to be the sole AST in S1 from skeletal (*23*), smooth (*27*, *28*), and *Dictyostelium* myosin (*26*). It is conserved in myosin and appears to be essential to energy transduction. We assume in all subsequent discussion that skeletal and cardiac S1 have one AST in Trp508 and that this residue is totally quenched by modification of SH1 with fluorescein.

We observed the enhancement, and changes in acrylamide quenching, of AST emission upon binding nucleotide or nucleotide analogue to S1. The AST fluorescence enhancement upon nucleotide (N) binding, $\Delta I(\mathrm{N})/\Delta I(-)$, is related to the quantum efficiency, ϕ, of the AST. When ΔI isolates solely the unperturbed AST emission (method 1), using fluorescein modification as perturbant,

$$\frac{\Delta I(\mathrm{N})}{\Delta I(-)} = \frac{\phi_{\mathrm{Trp508}}(N)}{\phi_{\mathrm{Trp508}}(-)} \qquad (2)$$

When ΔI isolates the combined perturbed and unperturbed AST emission (method 2), fluorescence enhancement depends on a more complicated combination of perturbed and unperturbed AST quantum efficiencies as derived elsewhere (*23*). The two kinds of fluorescence enhancement measurements detect related quantities by independent methods so that when both measurements are completed we relate all of them to the ratio of quantum efficiencies on the right-hand side of eq 2.

Acrylamide quenching of AST emission likewise has two forms depending on how AST emission is isolated. When ΔI isolates solely the unperturbed AST emission, using fluorescein modification as perturbant,

$$\frac{\Delta I_0}{\Delta I} = 1 + [Q]K_{\mathrm{Q}} \qquad (3)$$

where [Q] is quencher concentration, ΔI_0 is AST emission in the absence of quencher, and K_{Q} is the quenching constant of the unperturbed AST. When ΔI isolates the combined perturbed and unperturbed AST emission, quenching depends approximately on [Q] as in eq 3, but the proportionality constant defines the effective quenching constant, K_{eff}. K_{eff} depends on K_{Q} and AST quantum efficiencies as derived elsewhere (*23*). Measurements of K_{eff} and K_{Q} detect related quantities by independent methods so that when both measurements are completed we relate all of them to K_{Q}.

All acrylamide quenching data are plotted as a function of quencher concentration and fitted with a line in the form of eq 3 with K_{Q} as the free parameter using linear least squares.

Circular Dichroism. Near-ultraviolet circular dichroism (near UV CD) spectra were recorded in a 0.5-cm path length cell at 20 °C on a Jasco-715 spectropolarimeter (Tokyo, Japan). Protein spectra were measured with 20 μM S1, 0.5 mM $MgCl_2$, 60 mM KCl, and 30 mM HEPES, pH 7.0. Nucleotide concentrations were 0.125 mM for ADP, ATP or ATPγS (1 mM ATP for TNP-βS1). In samples containing ATP, an ATP regeneration system (5 μM pyruvate kinase, 8 mM phosphoenol pyruvate) was added to keep the ATP concentration constant. To obtain a spectrum from native S1, CD was recorded from a sample containing S1 with or without nucleotide or trapped nucleotide analogues, and subtracted from this was a similarly recorded spectrum from an identical mixture without the protein. To obtain a spectrum from probe-modified S1, CD was recorded in a 1-cm cell from a sample containing modified S1 with or without nucleotide or trapped nucleotide analogues, and subtracted from this was a similarly recorded spectrum from an identical mixture with native S1 substituting for the modified protein.

Fractional Concentration of Intermediates during ATPase. Myosin S1 forms transient intermediates with substrate during ATPase. Scheme 1 summarizes the principal intermediates where M is S1, A is actin, M*, M**, and M^ represent distinct myosin conformations, and A··· or A. implies weak or strong actin binding to myosin. In steady-state, the transient intermediates in the absence of actin (top row) are occupied at fractional concentrations that are known for a variety of myosins (*3*, *4*, *54*). Nucleotide analogues induce S1 structures imitating the transient intermediate conformations permitting the investigation of transient S1 structure with slow or time-independent techniques such as X-ray crystallography, CD, or steady-state fluorescence. Exhaustive study of the association of analogue-induced and transient intermediate S1 structures lead to the identification of bound ATPγS or trapped ADP·BeF_x (low ionic strength) with M*·ATP, trapped ADP·Vi or ADP·AlF_4^- or ADP·BeF_x (high ionic strength) with M**·ADP·P_i, and bound ADP with M^·ADP (*31*, *33*, *34*, *51*, *55*, *56*).

A structure sensitive signal, *F*, furnishes an estimate of the fractional concentrations of the transient intermediates during steady-state ATPase, even when *F* is not time-resolved, if the signal provides sufficient constraints. *F*, observed from S1 + MgATP, is compared to the same signal observed from S1, S1·ATPγS or S1·ADP·BeF_x (low ionic strength), S1·ADP·AlF_4^- or S1·ADP·Vi, and S1·ADP, mimicking the ATPase intermediates, M, M*, M**, and M^, respectively. This method was demonstrated for various signals including near UV CD spectra, and fluorescence intensity and quenching data (*23*, *33*). In addition to these established applications, herein we apply the method to CD signals induced in the absorption band of probes attached to S1.

RESULTS

Proteolysis of βS1. Figure 2 shows the SDS−PAGE separation of protein fragments produced by the tryptic digestion of S1 and βS1 and the mixture of the two, lanes 5, 7, and 6, respectively. Trypsin splits the heavy chains of both myosin S1's at two points, loops 1 and 2, producing the characteristic 25, 50, and 20 kDa fragments (*8*, *10*). The T-βS1 25- and 20-kDa fragments (β25k and β20k) are

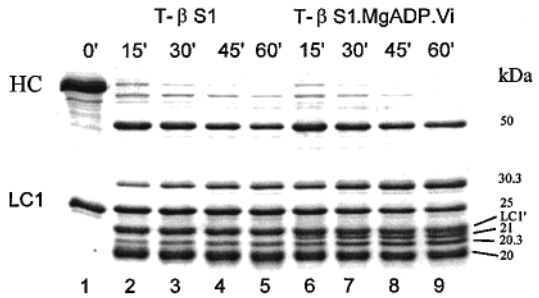

FIGURE 4: SDS−PAGE of the tryptic digest of βS1 (T-βS1) and the stable vanadate trapped complex βS1·MgADP·Vi (T-βS1·ADP·Vi). Abbreviations are as in Figure 2. Lane 1 contains intact βS1. Lanes 2−5 show the time-dependent digestion of βS1 in the absence of nucleotide. Lanes 6−9 show the time-dependent digestion of βS1·Mg·ADP·Vi. Samples were digested with a 1:50 w/w ratio of trypsin:βS1 for 15, 30, 45, and 60 min. Digestion of the βS1·Mg·ADP·Vi trapped complex was performed after removal of the free MgADP and vanadate.

Scheme 2

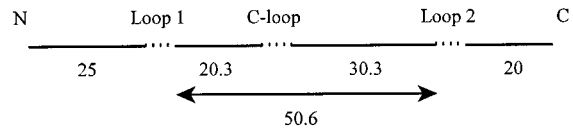

indistinguishable from the corresponding skeletal T-S1 fragments (S25k and S20k). The T-βS1 50-kDa fragment (β50.6k) migrates slightly more slowly than the skeletal 50 kDa (S50k) (see lane 6 Figure 2). Two new fragments were detected in the cardiac digest having molecular masses of ~30 and ~20 kDa (β30.3k and β20.3k) as determined by comparison with standard molecular weight markers (lane 8) or the 20-kDa fragment of T-S1. All molecular weights of the peptides were calculated based on the relative SDS−polyacrylamide gel electrophoretic mobility.

The origin of β20.3k and β30.3k was investigated by following the tryptic digestion of the βS1 in time (Figure 4 lanes 1−5). There the appearance of the new fragments parallel the disappearance of β50.6k. Quantitative analysis of lanes 1−5 using gel scanning (appendix) showed that the summed total absorbance from the β50.6k, β20.3k, and β30.3k bands remains constant in time, suggesting the two lighter peptides have a common origin in β50.6k. We identified the cutting point within β50.6k by sequence analysis of the N-termini of the β20.3k and β30.3k peptides yielding EQATGKGTLEDQI and EEQAEPD. These sequences line up with those of the human β-cardiac sequence beginning at Asp208 and Glu370 (*1*). Scheme 2 summarizes the linear structure of the βS1.

The start of the β20.3k peptide is at the location of the highly variable loop 1 and shows sequence identity with human βS1 starting only from Gly212 (GKGTLEDQI), where a known homology region among the myosin family begins (*57*). The residues preceding Gly212 are unique to bovine βS1 and were not previously reported. Starting from Arg369 bovine and human βS1, chicken, and skeletal S1 have identical sequences but are not part of a high sequence homology region in myosin. From the skeletal myosin crystal structure (Figure 1), Arg369 resides on a surface loop we refer to as the cardiac- or C-loop.

The effect of bound nucleotide (ATP or ADP) or trapped nucleotide analogue (ADP·Vi) on the tryptic digestion of βS1 was studied. Figure 4 shows the tryptic digest of βS1 without nucleotide (lanes 2−5) as compared to βS1·ADP·Vi (lanes 6−9). The trapped analogue did not change the main fragmentation pattern, although the rate for the production of the β30.3k fragment was accelerated, showing that the trapped analogue influences the accessibility of the C-loop to trypsin. Bound nucleotides (ATP or ADP) had a similar but smaller influence on C-loop accessibility to trypsin. Active site occupation by ATP, ADP, or ADP·Vi caused degradation of the β25k to β21k. In skeletal S1, nucleotide-induced degradation of S25k to S21k proceeds more rapidly and is also accompanied by degradation of the S50k to a 47-kDa fragment (*58*−*60*).

Figure 3 shows the SDS−PAGE separation of protein fragments produced by the tryptic digestion of βS1 in the absence (lanes 2−4) and presence of actin (lanes 5−7). Actin protects β50.6k from degradation into the β30.3k and β20.3k products by inhibiting the cut at Arg369. In skeletal S1, actin inhibits the proteolytic cut at loop 2 joining the S50k and S20k fragments (*14*, *15*). In βS1, actin fails to protect cleavage of the N-terminus of loop 2 as shown previously (*8*); however, the β20k produced from actoβS1 is slightly heavier than the fragment produced from βS1. This is shown by the digestion of F-βS1 in the absence (lane 9) and presence (lane 10) of actin and suggests actin binding at loop 2 lies after the cleavage point in actoβS1. Actin binding does not affect degradation of β25k to β21k due to the presence of the occupation of the active site by ADP (data not shown).

Limited trypsinolysis of skeletal myosin clipped the S1 at loops 1 and 2 and did not effect the Mg^{2+}-, Ca^{2+}- or K^+-EDTA-ATPase activities (*14*, *15*, *61*). Similar studies were performed on βS1 with results summarized in Figure 5. At time zero, trypsin and βS1 were combined. Aliquots withdrawn from the mixture at the time points shown in the figure had the digestion halted by addition of trypsin inhibitor and then were divided into two parts. From part 1, we quantitatively determined the fractional concentrations of the peptide fragments in the digest using SDS−PAGE and gel scanning (see appendix). From part 2, we measured the Mg^{2+}-, Ca^{2+}-, and K^+EDTA-ATPases. In Figure 5, open symbols pertain to ATPases and closed symbols to the fractional concentration of split βS1 species.

Figure 5A shows the ATPases, the fractional concentrations of βS1 split at loops 1 and 2 (βS1(1,2),▲) or at loops 1, 2, and the C-loop (βS1(1,C,2),◆), and the total absorption from β50.6k, β30.3k, and β20.3k (■), from a rapidly digested βS1 (1:50 trypsin:βS1). The K^+EDTA-ATPase (□) remains constant then gradually declines in correlation with the total absorption suggesting the digestion of βS1 beyond cuts at loops 1, 2, and the C-loop results in the inhibition of K^+-EDTA-ATPase. Consequently, we normalized the Mg^{2+}- and Ca^{2+}-ATPases with the K^+EDTA-ATPase to remove changes in these quantities due to the production of digestion products that do not split ATP. The normalized Mg^{2+}- (△) and Ca^{2+}-ATPases (◇) are shown in Figure 5A. The quantitative gel scans, upon which the fractional concentrations of βS1(1,2) and βS1(1,C,2) depend, are also corrected for contributions from the nonfunctional digestion products. Therefore, the fractional concentrations of βS1(1,2) and βS1(1,C,2) sum to 1 except at time zero where only βS1 is present.

Figure 5B shows the ATPases and the fractional concentrations of species during the initial fragmentation of βS1

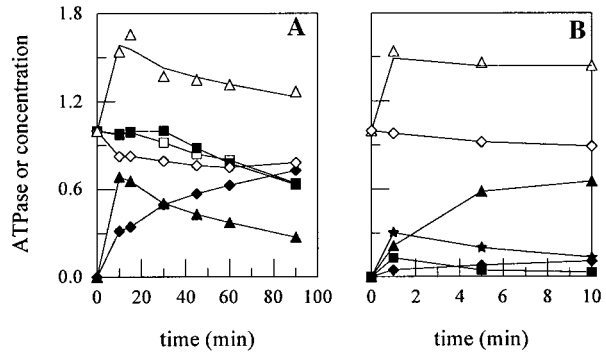

FIGURE 5: Fractional concentration of species and ATPase activity during trypsinolysis. (A) Closed symbols represent fractional concentrations of βS1 split by tryptic digestion at loops 1 and 2 (βS1(1,2), ▲) or at loops 1, 2 and the C-loop (βS1(1,C,2), ◆), and the total absorbance (normalized to 1 at time zero) from βS1, βS1-(1,2), and βS1(1,C,2) (■) as a function of time after the start of the digestion. The fraction concentrations of βS1(1,2) and βS1-(1,C,2) sum to 1 and represent all of the βS1 present in solution except at zero time when only native βS1 was present. Digestion was performed with a 1:50 w/w ratio of trypsin:βS1. Fractional concentrations and total absorbance were computed as described in the appendix from the quantitative analysis of Coomassie stained bands on SDS−PAGE gels. Open symbols represent the Mg^{2+}-ATPase (△), Ca^{2+}-ATPase (◇), and K^+EDTA-ATPase (□) of the digest in solution. The time zero value of the ATPases is equal to that from the native βS1 normalized to 1. A solid line joins observed points except for the Mg^{2+}-ATPase where it was computed from a weighted sum of the fractional concentration of split species according to eq 4. (B) Experiments similar to those in (A) but on a shorter time scale and performed with a 1:200 w/w ratio of trypsin:βS1 such that the heavy precursors to β50.6k can be observed. Closed symbols represent the fractional concentration of the split βS1 species, βS1(1) (■), βS1(2) (★), βS1(1,2) (▲), and βS1(1,C,2) (◆). The fractional concentration of the native βS1 species (not shown) was 1 at time zero and decreased to < 0.1 after 5 min. Open symbols represent the ATPases as in panel A.

Scheme 3

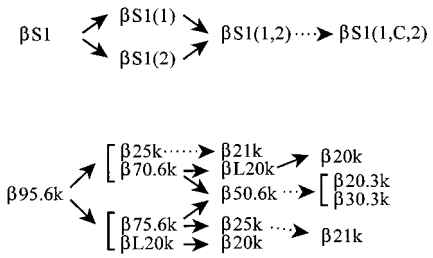

(1:200 trypsin:βS1), wherein the heavy precursors (β70.6k or β75.6k) to the β50.6k fragment can be observed. In these experiments, no significant time dependence in the K^+EDTA-ATPase (data not shown) indicates no production of non-functional digestion products. The fractional concentrations of βS1 split at loop 1 (βS1(1),■) or loop 2 (βS1(2),★), βS1-(1,2) (▲), and βS1(1,C,2) (◆) are plotted. Only βS1 is present at time zero and its contribution drops to less than 10% within 5 min. We found βS1(2) and βS1(1) are in roughly a 2:1 molar ratio during the initial fragmentation of βS1. Alternatively, mild tryptic digestion of βS1 was shown to produce β75.6k and β70.6k with equal probability under different pH and ionic strength conditions (*8*).

Scheme 3 summarizes these findings for production of the split βS1 species (top) and proteolytic fragments observable with electrophoresis (bottom). The broken arrow implies the nucleotide affects the rate of proteolysis. Cutting at loop 2 produced a slightly higher molecular weight fragment (long β20k or βL20k) that shortened to a stable β20k as proteolysis progressed (see appendix).

Correlation of the Mg^{2+}- and Ca^{2+}-ATPases with the fractional concentrations of the various forms of the split βS1 indicates the effect of the cutting of the peptide backbone at loop 1, 2, or the C-loop on ATPase. In Figure 5A, after an initial decrease, the Ca^{2+}-ATPase remains nearly constant throughout the digestion. The Mg^{2+}-ATPase dramatically increases initially then declines to an intermediate value. In Figure 5B, similar trends in the Ca^{2+}- and Mg^{2+}-ATPase are recognized where the βS1(1) and βS1(2) species also contribute to the ATPase. ATPase data in Figure 5 are accounted for by a sum over the fractional concentrations of βS1, βS1(1), βS1(2), βS1(1,2), and βS1(1,C,2) with each species weighted by its specific ATPase according to eq 4

$$\text{ATPase} = \beta\text{S1} + a_1\beta\text{S1(1)} + a_2\beta\text{S1(2)} + a_{1,2}\beta\text{S1(1,2)} + a_{1,C,2}\beta\text{S1(1,C,2)} \quad (4)$$

where a_i's are the specific rates normalized such that intact βS1 has the specific rate of 1. We find that for the Mg^{2+}-ATPase, $a_1 \approx a_{1,2} \approx 1.6-2.0$ and $a_2 \approx a_{1,C,2} \approx 1.0-1.2$, implying that the cut at loop 1 activates, while the cut at loop 2 has little effect on, the Mg^{2+}-ATPase. Mg^{2+}-ATPase activation by the loop 1 cut is reversed by the C-loop cut. The similar analysis for the Ca^{2+}-ATPase shows that all split species have a specific ATPase rate of ~0.8. The solid lines following the time course in the Mg^{2+}-ATPases in Figure 5 are fitted using eq 4 and the specific rates mentioned above.

Formation and Stability of βS1 Nucleotide Analogue Complexes. Skeletal S1 forms stable trapped complexes with nucleotide analogues resulting in the inhibition of ATPase activity that is fully reversible upon trap release (*51*, *55*, *62*, *63*). We monitored nucleotide analogue trap formation and dissociation in skeletal and cardiac S1 with the time-dependent change in the myosin ATPase. Scheme 4 models the trapping mechanism, where A is actin and PA is the phosphate analogue. Differing S1 conformations of interest in this scheme are identified by $S1^\dagger$ and $S^\ddagger$. $S1^\dagger$ is characteristic to the PA and mimics particular and known ATPase transient intermediates (*31*, *33*, *51*, *55*, *56*). Actin binding to $S1^\dagger$·ADP·PA forms A···$S1^\ddagger$·ADP·PA, a reversible intermediate with loosely bound PA such that the ADP·PA complex is readily displaced by ATP. We associate A···$S1^\ddagger$·ADP·PA with the weak actin binding states in Scheme 1.

Trap formation and spontaneous dissociation involves the first three steps in Scheme 4 while actin-induced dissociation involves steps 4 and 5. Appropriately chosen initial conditions allows separate observation of these processes. ATPase inhibition monitors solely the concentration of $S1^\dagger$·ADP·PA because it contains the only bound nucleotide in Scheme 1 that is not displaced by ATP. Consequently, the presence of the other intermediates is surmised indirectly and/or with the use of additional information from other experiments.

We study the kinetics of trap formation by the addition of PA to a mixture of MgADP and S1. Steps 1 and 2, with equilibrium constants $K_1 = k_{+1}/k_{-1}$ and $K_2 = k_{+2}/k_{-2}$, are in quasi-equilibrium on the time scale of trap formation due to their rapid forward and reverse rates (*54*, *63*, *64*). They influence trap formation through only their equilibrium constants. Given $K_1 \approx 1-3 \times 10^5$ M^{-1} (*65*, *66*), the unknowns governing trap formation are K_2 and the step 3

Scheme 4

$$\mathrm{S1+ADP} \underset{k_{-1}}{\overset{k_{+1}}{\rightleftharpoons}} \mathrm{S1.ADP+PA} \underset{k_{-2}}{\overset{k_{+2}}{\rightleftharpoons}} \mathrm{S1.ADP.PA} \underset{k_{-3}}{\overset{k_{+3}}{\rightleftharpoons}}$$

$$\mathrm{S1^{\dagger}.ADP.PA+A} \underset{k_{-4}}{\overset{k_{+4}}{\rightleftharpoons}} \mathrm{A\cdots S1^{\ddagger}.ADP.PA} \underset{k_{-5}}{\overset{k_{+5}}{\rightleftharpoons}} \mathrm{A.S1+ADP+PA}$$

forward and backward rates k_{+3} and k_{-3}. The observed stability of trapped S1 (see below) is such that k_{-3} does not significantly influence trap formation, and it can be neglected. We determined K_2 and k_{+3} by nonlinear fitting of the observed time-dependent ATPase inhibition due to stable trap formation for 0.05, 0.2, and 0.4 mM PA (only 0.2 and 0.4 mM for the AlF_4^- phosphate analogue) with theoretical curves generated numerically from the coupled ordinary differential equations modeling the Scheme 4 reaction for zero actin concentration. Time zero ATPase was equal to control untrapped S1 and normalized to 100%. We surmised initial guesses for K_2 and k_{+3} for use in the nonlinear routines from the Michaelis-Menton double reciprocal plots of phosphate analogue concentration versus the observed pseudo first-order rate of ATPase inhibition (*51*).

Spontaneous trap dissociation relaxation time is on the order of days at low temperature (*51*, *62*). We observed the first hour of the ATPase recovery at room temperature due to the spontaneous trap dissociation, the initial rate of recovery, from an initial condition wherein $S1^{\dagger}$·ADP·PA was the only component present. The initial rate of ATPase recovery due to spontaneous trap dissociation depends solely on k_{-3}. The value of k_{-3} was found by nonlinear fitting of the observed time-dependent ATPase recovery with theoretical curves generated as described above.

Actin-induced trap dissociation is rapid as compared to spontaneous dissociation and depends on the equilibrium constant K_4 and the forward rates k_{+4} and k_{+5}. Step 5 is irreversible under our experimental conditions. We observed the ATPase recovery due to actin-induced trap dissociation from an initial condition wherein $S1^{\dagger}$·ADP·PA and actin are the only components present. The values of K_4, k_{+4}, and k_{+5} were found by nonlinear fitting of the observed time-dependent ATPase recovery with theoretical curves generated as described above except for the presence of 10 μM actin. The actin-induced release of the BeF_x analogue happens in one apparent step prohibiting any distinction between the actin binding step and PA release. The sole PA release rate for BeF_x may be expressed as either k_{+4} or k_{+5}, but these two parameters are dependent.

Figure 6 shows the ATPase relaxation in βS1 for the BeF_x, Vi, and AlF_4^- phosphate analogues for all the processes discussed above. These data constrain the family of theoretical curves, shown in solid lines, from which K_2, k_{+3}, k_{-3}, K_4, k_{+4}, and k_{+5} are estimated (either k_{+4} or k_{+5} for BeF_x). The estimates for these kinetic constants are summarized in Table 1. Table 1 includes comparable constants for skeletal S1 observed here or taken from the literature (*51*). Cardiac and skeletal S1 show nearly identical trends for the various parameters, although absolute values are often divergent. The apparent two step actin-induced dissociation of the M** mimicking analogues Vi and AlF_4^- in S1 and βS1 suggests the existence of a reversible actin bound ATPase intermediate

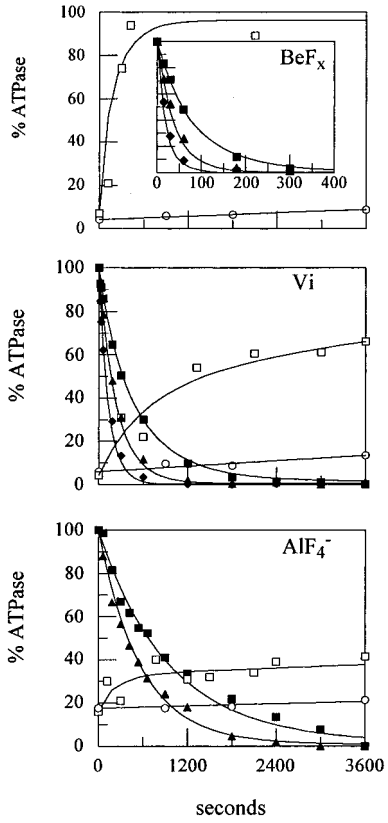

FIGURE 6: ATPase relaxation for βS1 and the BeF_x (top), Vi (middle) and AlF_4^- (bottom) phosphate analogues. ATPase inhibition accompanies trap formation for analogue concentrations of 50 (■), 100 (▲), and 200 (◆) mM [200 (■) and 400 (▲) mM for AlF_4^-]. ATPase recovery occurs spontaneously (○) or as a result of actin binding (□). Actin-induced ATPase recovery curves for the Vi and AlF_4^- phosphate analogues were recorded for an additional 2 h (10800 s total) reaching ~90 and ~50% of control ATPase, respectively.

following M** (*67*). This actin-bound intermediate has a position in the ATPase scheme akin to the weak binding state of the myosin cross-bridge in a muscle fiber (*36*, *68*), possibly resembling A···M**·ADP·P_i from Scheme 1. Unlike the M** analogues, actin binding releases the M* mimicking analogue BeF_x in S1 and βS1 in one apparent step.

AST Fluorescence in Myosin. Table 2 compares the enhancement of total tryptophan fluorescence due to nucleotide binding or the trapping of nucleotide analogues for skeletal and cardiac S1. Bound nucleotides and trapped nucleotide analogues enhance fluorescence in both forms of S1 by roughly equivalent amounts.

Figure 7 shows the acrylamide quenching of Trp508 fluorescence in βS1 (●), βS1+MgATP (▲), βS1.ADP (○), βS1·ADP·BeF_x (■), and βS1·ADP·AlF_4^- (◆). Trp508 emission isolation was accomplished by formation of ΔI in

Table 1: Kinetic Parameters for Phosphate Analogue Trapping and Release[a]

	K_2 (M^{-1})		k_{+3} (s^{-1})		$k_{-3} \times 10^5$ (s^{-1})		$K_4 \times 10^{-4}$ (M^{-1})		k_{+4} ($M^{-1}s^{-1}$)		$k_{+5} \times 10^4$ (s^{-1}) [b]	
PA	S1	βS1	S1	βS1	S1	βS1	S1	βS1	S1	βS1	S1	βS1
BeF_x	1698	831 ± 235	0.065	0.38 ± 0.09	0.1	1.4 ± 0.08	>500	>500	276 ± 64	800 ± 157	~14−28	~40−80
Vi	12500	1700 ± 294	0.008	0.032 ± 0.004	0.2	2.3 ± 0.3	17 ± 6	13 ± 8	375 ± 140	91 ± 35	7.9 ± 2.9	3.4±2.0
AlF_4^-	7518	1260 ± 523	0.004	0.0054 ± 0.0016	0.4	1.2 ± 0.3	11 ± 4	3.0±0.5	79 ± 20	121 ± 60	2.5 ± 1.6	0.64 ± 0.42

[a] Skeletal S1 values for K_2, k_{+3}, and k_{-3} are from Werber et al., (*51*) at 0 °C (spontaneous decomposition, k_{-3}) and 20 °C (complex formation, K_2 and k_{+3}). Skeletal S1 experiments determining K_4, k_{+4}, and k_{+5} (actin-induced decomposition) and all βS1 experiments were conducted at 20 °C. Standard deviations were estimated from nonlinear least squares minimization (*89*). [b] Either k_{+4} or k_{+5} (but not both) can be estimated for the BeF_x analogue because step 4 in Scheme 4 is apparently irreversible making the distinction between A···S1‡·ADP·PA and A·S1 impossible. Equivalent to expressing the release rate as $k_{+4} \approx 800\ M^{-1}\ s^{-1}$ is $k_{+5} \approx k_{+4}[A] \approx 800 \times (5-10) \times 10^{-6}\ s^{-1} = 0.004-0.008\ s^{-1}$, where $[A] \approx (5-10) \times 10^{-6}$ M is the average free actin concentration.

Table 2: Total Tryptophan Fluorescence Enhancement upon Nucleotide Binding or Nucleotide Analogue Trapping[a]

		$[I(S1 + N) - I(S1)]/I(S1)$	
transient	analogue (N)	skeletal	cardiac
M*	ADP·BeF_x	26.1 ± 1.2	24.8 ± 2.0
M**	ADP·AlF_4^-	37.7 ± 1.0	29.3 ± 2.0
M^	ADP	10.2 ± 2.0	6.7 ± 1.2
MgATP		31.2 ± 1.0	28.5 ± 1.0

[a] Myosin transient designation is from Scheme 1. The fluorescence increment, $[I(S1 + N) - I(S1 + N')]/I(S1 + N') = \gamma(N, N')$, for $\gamma(N,-)$ expressed as % where $I(S1 + N)$ is the total tryptophan fluorescence from skeletal or cardiac S1 with nucleotide or nucleotide analogue, N. Errors shown are standard error of the mean with 3−4 observations. Sometimes the fluorescence increment γ(N,ADP) is computed. The two expressions are related by $\gamma(N, N') = [\gamma(N,-) - \gamma(N',-)]/\gamma(N',-) + 1$.

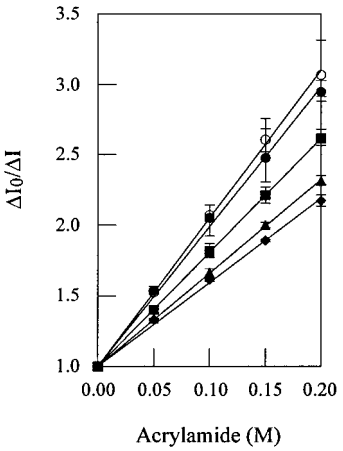

FIGURE 7: Acrylamide quenching of Trp508 fluorescence in βS1 (●), βS1+MgATP (▲), βS1·ADP (○), βS1·ADP·BeF_x (■), and βS1·ADP·AlF_4^- (◆). Trp508 emission was isolated using the difference of intensities between βS1 and F-βS1 (method 1).

eq 1 with fluorescein modifying SH1 in the perturbed protein (method 1). The slope of these curves is the acrylamide quenching constant, K_Q. Similar data were acquired when Trp508 emission isolation was accomplished by formation of ΔI with the nucleotide perturbants (method 2, data not shown). Table 3 summarizes the quenching data, and the Trp508 fluorescence enhancement due to nucleotide binding or trapping of nucleotide analogues, for the various nucleotide bound or trapped states of βS1. Most quantities were measured using the two different methods (1 and 2) for the isolation of Trp508 emission. Table 3 also compares the acrylamide quenching constant, K_Q, for skeletal and cardiac S1.

Data in Table 3 indicate the vicinity of Trp508 undergoes conformational change induced by the various nucleotides or nucleotide analogues bound to the active site of βS1, as observed previously for skeletal S1 (*22*, *52*, *53*). Quenching constants for skeletal and cardiac S1 are similar in absolute value and follow the identical correlation with the active site occupant such that K_Q is the largest without nucleotide or with bound ADP, the smallest with trapped ADP.AlF_4^-, and similar to that during steady-state hydrolysis of MgATP and intermediate to ADP and ADP·AlF_4^- with trapped ADP·BeF_x at low ionic strength. With skeletal S1, K_Q measures the accessibility of Trp508 to collisional quenching. The similarity of the quenching results between skeletal and cardiac S1 suggest that K_Q has the same meaning in βS1. If identical Trp508 acrylamide quenching mechanisms are at work in S1 and βS1, the range of K_Q's in Table 3 indicate the neighborhood of Trp508 in βS1 undergoes less dramatic conformational change than the corresponding region in skeletal S1, for the analogues investigated. As these analogues mimic the transient conformations in S1 during ATP hydrolysis, we make the identical conclusion about the neighborhood of Trp508 in βS1 during ATPase.

Quantum efficiencies for Trp508 in βS1 are in good agreement when computed by methods 1 and 2. The K_Q's computed by methods 1 and 2 do not agree to within experimental error. K_Q values derived with method 2 are larger that those from method 1 except with ADP bound. The reason for the incompatibility of the two methods regarding quencher accessibility is under investigation. This kind of discrepancy was not observed in skeletal S1 (*23*).

The comparison of the fluorescence enhancements and quenching constants from bound or trapped nucleotide analogues to that observed in the presence of MgATP indicate the fractional concentration of the transient intermediates in myosin during ATPase. These findings, listed in the last column of Table 3, are discussed in the section on the fractional concentration of ATPase intermediates.

CD Spectra from Native and Probe-Modified Myosins. The near UV CD spectrum of skeletal (●) and cardiac S1 (○), as compared in the upper panel of Figure 8, differ throughout the near UV region where the aromatic side chains absorb and in particular at wavelengths > 295 nm where tryptophan absorbs exclusively (*33*). Cardiac S1 without nucleotide and with bound nucleotides or trapped nucleotide analogues are also compared in Figure 8. Besides the S1 and βS1 without substrate, the upper panel has the M** analogue ADP·AlF_4^- trapped βS1 (■) and βS1+MgATP (▲) in steady-state. The lower panel has the M* analogues ATPγS (◇) bound and

Table 3: Fluorescence Enhancement and Acrylamide Quenching of Trp508 in Cardiac S1[a]

		$\phi_{508}(N)/\phi_{508}(-)$		K_Q[b]		fractional concentration	
transient	analogue (N)	method 1	method 2	method 1	method 2	method 1	method 2
M		1		9.9 ± 0.30 /10.5			
M*	ADP·BeF_x	1.55 ± 0.03	1.35−1.91	8.1 ± 0.20 /7.5	8.71−9.08	0−0.33	0.17−0.26
M**	ADP·AlF_4^-	1.94 ± 0.09	1.61−2.26	6.0 ± 0.15 /5.6	6.89−7.22	0.67−0.86	0.72−0.79
M^	ADP	1.23 ± 0.08	1.15−1.31	10.4 ± 0.54/9.3	9.00−9.60	0−0.22	0−0.09
MgATP		1.90 ± 0.03	1.54−2.16	6.6 ± 0.06 /6.4	7.34−7.64		

[a] Trp508 emission was isolated from βS1 by the use of eq 1 with fluorescein (method 1) or nucleotide (method 2) perturbants. Errors shown as ± are standard error of the mean with 2−6 observations. Value ranges are listed for computed quantities with any number within the range equally likely. [b] K_Q measured with method 1 is shown for cardiac/skeletal S1.

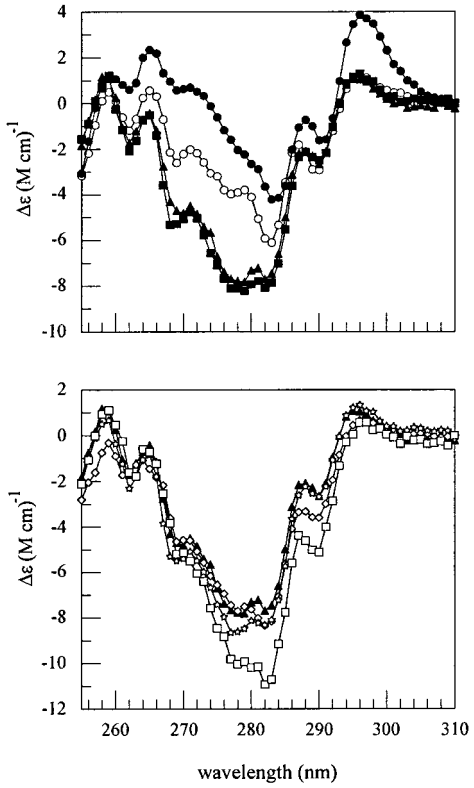

FIGURE 8: Near UV CD spectra from myosin S1. Upper panel: cardiac (○) and skeletal S1 (●) without nucleotide, and the M** analogue ADP·AlF_4^- trapped βS1 (■). Lower panel: M* analogues ATPγS (◇) bound and ADP·BeF_x (☆) trapped βS1, and the M^ analogue ADP (□) bound βS1. For comparison, βS1+MgATP (▲) in steady-state is plotted in both panels.

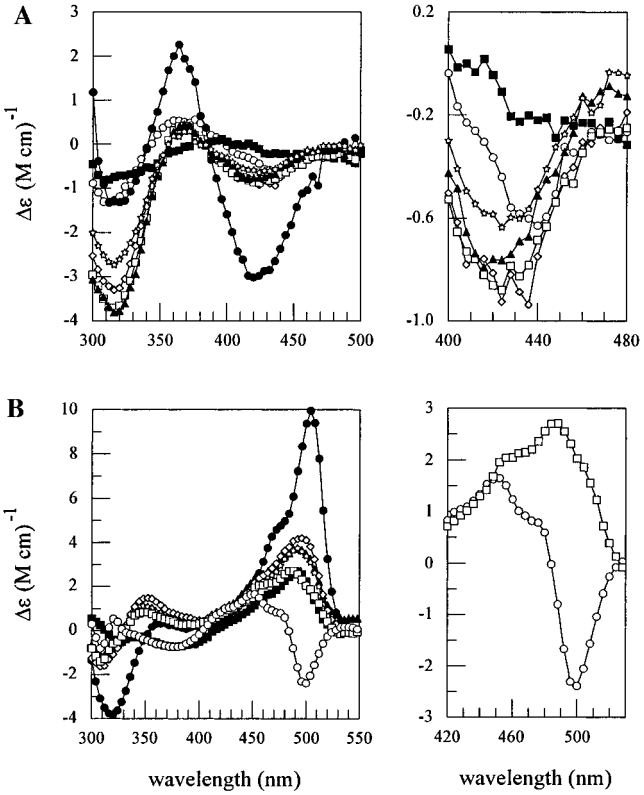

FIGURE 9: Protein induced CD spectra from probes of interface I and II. Selected spectra from the left panel are replotted and rescaled in the right panel for reasons described in the text. (A) Spectra from TNP modifying RLR (interface II) in myosin. Spectra shown are from no nucleotide TNP-βS1 (○) and TNP-S1 (●), the M* analogues ATPγS (◇) bound and ADP·BeF_x (☆) trapped TNP-βS1, the M** analogue ADP·AlF_4^- trapped TNP-βS1 (■), the M^ analogue ADP (□) bound TNP-βS1, and TNP-βS1+MgATP (▲) in steady-state. (B) Spectra from fluorescein modifying SH1 (interface I) in myosin. Symbols for spectra shown are same as in (A) with F replacing TNP.

ADP·BeF_x (☆) trapped βS1, the M^ analogue ADP (□) bound βS1, and βS1+MgATP (▲) in steady-state. The upper panel shows the similarity between the βS1·ADP·AlF_4^- and βS1+MgATP spectra expected for an analogue mimicking M**, the predominant ATPase intermediate at 20 °C, and the large difference between βS1 and the other spectra shown. The lower panel shows that similarity of the M* analogues, βS1·ATPγS and βS1·ADP·BeF_x, their overlap with βS1+MgATP, and the rather large difference between βS1·ADP and the other spectra.

Figure 9A (left) shows the protein-induced CD spectra of trinitrophenylated skeletal (●) and cardiac S1 (○) at the three lowest absorption bands of the RLR bound probe. TNP modifies RLR in skeletal and cardiac S1 and occupies a site at the interface of the catalytic and lever arm domains (Figure 1) (*29*, *30*). The signal of TNP-βS1 has a smaller amplitude but similar shape to that of skeletal TNP-S1 owing in part to the change in the residue neighboring RLR from Tyr (skeletal) to Phe (cardiac) (*45*). The CD spectra of TNP-βS1 complexed with substrates and analogues are shown with symbols identical to those in Figure 8. The spectra are distinct for the different analogues but show less contrast than the CD signals from native (Figure 8) or fluorescein-labeled βS1 (Figure 9B) under identical conditions.

Figure 9B (left) shows the protein-induced CD spectra of F-S1 (●) and F-βS1 (○) at the two lowest absorption bands of the SH1 probe. Fluorescein modifies SH1 in skeletal and cardiac S1 and occupies a region near the switch II helix at Trp508 (Figure 1) (*29*, *30*). These spectra sharply contrast in the lowest energy band where they differ in sign (*30*). Evidently, the fluorescein probe maintains very different

Table 4: Fractional Concentration of ATPase Transient Intermediates of S1 and Modified S1[a]

		native		RLR-modified [b]		SH1-modified [b]	
transient	analogue	S1	βS1	TNP-S1	TNP-βS1	F-S1	F-βS1
M		0+0.1	0+0.04	0 (0)+0.04	0 (0)+0.11	0.09 (0.14) ± 0.02	0.06 (0) ± 0.04
M*	ATPγS	0.14 ± 0.11	0 + 0.17	0.3 (0.4) ± 0.12	0.4 (0.6) ± 0.11	0.56 (0.47) ± 0.03	0.82 (1) ± 0.12
M**	ADP·AlF_4^-	0.85 ± 0.10	0.79 ± 0.19	0.1 (0.1) ± 0.08	0 (0)+0.10	0 (0)+0.02	0.13 (0) ± 0.03
M^	ADP	0+0.08	0.12 ± 0.03	0.6 (0.5) ± 0.11	0.4 (0.5) ± 0.11	0.35 (0.39) ± 0.02	0 (0)+0.14

[a] Columns of fractional concentrations not adding to 1 contain an unassigned component. Errors are standard deviations. [b] Values in parentheses were obtained when the M* transient was mimicked with trapped ADP·BeF_x at low ionic strength.

conformations in the probe binding cleft of the two proteins. The binding of nucleotides and analogues dramatically changed the shape of the spectrum and have signals that are distinct for each nucleotide and analogue. Symbols representing the spectra for the different states of the F-βS1 are identical to those in Figure 8. Fluorescein CD is sensitive to protonation/deprotonation of the xanthene group with the protonated form having a blue-shifted absorbance. Evidence for the presence of these two species in the fluorescein-modified βS1 is the prominence of the 460 nm shoulder on the main absorbance peak at 500 nm. The spectrum from F-βS1·ADP (Figure 9B, right) has a prominent shoulder at 460 nm, but the most dramatic demonstration of the presence of two bound forms of fluorescein comes from the no nucleotide spectrum of F-βS1. Without nucleotide, the bound probe assumes two very different conformations in the βS1 for its protonated and deprotonated forms that give oppositely signed CD signals. This effect carries over to the absorbance band at 320 nm where the no nucleotide spectrum is again split into two oppositely signed signals.

The comparison of the bound or trapped nucleotide analogue spectra with spectra measured in the presence of MgATP indicate the fractional concentration of the transient intermediates in myosin during ATPase for the native and probe-modified βS1. These findings are discussed in the next section.

Fractional Concentration of Intermediates during ATPase. During ATPase, myosin S1 forms transient intermediates summarized by the upper pathway of Scheme 1. Trp508 emission enhancement and acrylamide quenching distinguish the different intermediates sufficiently to permit their fractional contribution to the equivalent quantities observed from S1+MgATP to be recognized. We determined the fractional concentration of the intermediates in S1+MgATP for rabbit skeletal S1 (*23*) and herein perform the same determination for βS1.

The fractional contributions of transient intermediates to the fluorescence properties of Trp508 in βS1+MgATP are listed in Table 3. Fractional concentration estimates from the fluorescence data are unambiguous if we assume that there is no contribution from state M, the no nucleotide intermediate. This assumption is reasonable for the nucleotide concentration in the observed S1+MgATP system and supported by subsequent findings using CD where there are sufficient constraints to make an experimental determination of the concentration of M. Estimates were made for each of the methods (1 and 2) for isolating Trp508 emission. We find that M** is the predominant intermediate in S1+MgATP for either method with a fractional concentration of 0.7−0.9. The two methods differ on how they divide the remainder of the fractional occupancy between the M* and M^ intermediates. Method 1 shows no preference between them, but method 2 indicates the remainder occupies M*. The S1·ADP·BeF_x complex is known to have roughly equal contributions from M* and M** conformations at 60 mM KCl in skeletal S1 (*34*). This possibility, considered when computing the fractional concentrations for βS1, had only the effect of raising the upper limit on the M** contribution. Values listed in Table 3 assume the S1·ADP·BeF_x complex to be exclusively an M* analogue.

The near UV CD spectrum of S1+MgATP in the steady-state, from Scheme 1, is the sum of spectra from the M, M*, M**, and M^ intermediates with weighting factors equal to their fractional concentration. Modeling the CD spectra from the intermediates by spectra measured from the corresponding analogue-induced S1 conformation, then calculating their fractional contribution to the spectrum from S1+MgATP, we should obtain the transient intermediate fractional concentrations. We determined the fractional concentration of the intermediates in S1+MgATP for rabbit skeletal S1 (*33*, *34*) and herein perform the same determination for βS1 and the probe-modified forms of S1 and βS1. Table 4 summarizes the results.

In native proteins, the near UV CD spectrum of S1+MgATP is compared to model spectra for the fractional concentration calculation (βS1 spectra are from Figure 8). Native skeletal and cardiac S1 results, compared in Table 4, show that both species have M** as the predominant intermediate with the remainder of the fractional occupancy in the M* or M^ intermediates, respectively. Different skeletal and cardiac, second-most-populated intermediates, is not a statistically significant observation. The next column contains identical quantities computed from TNP-modified protein (TNP-βS1 spectra are from Figure 9A). CD spectra from TNP-modified S1's cover the 300−500 nm wavelength domain; however, analogue induced structures are best able to model the ATPase transient structures at the lowest energy transition centered at ~425 nm (see Figure 9A, right). The fractional concentrations are calculated using spectral shapes in the 400−500 nm wavelength domain. TNP-S1 and TNP-βS1 have similar transient intermediate distributions where M* and M^ are about equally populated and account for practically all of the population density. TNP modification of S1 increases the steady-state Mg^{2+}-ATPase 8-fold in skeletal and 4-fold in cardiac S1 implying the redistribution of the transient intermediates is achieved by diminishing the stability of M** to below that of M* and M^. Our findings are also consistent with a reduced (but not negligible) phosphate burst. TNP-S1 was shown previously to have a negligible phosphate burst (*69*) and characteristic absorption spectra (*70*, *71*) both suggesting M* is the predominant

intermediate in TNP-S1+MgATP, in rough agreement with the present findings.

The final column of Table 4 contains intermediate fractional concentrations in fluorescein-modified protein (F-βS1 spectra are from Figure 9B). CD spectra from fluorescein-modified S1's cover the 300−550 nm wavelength domain where the two lowest energy transitions in the fluorescein absorb. F-S1 and F-βS1 have intermediate distributions where the predominant state has shifted from M** to M*. Fluorescein modification of SH1 increases the steady-state Mg^{2+}-ATPase 2.1-fold in skeletal and 2.8-fold in cardiac S1, implying the modification diminishes the stability of M** to below that of M*. Our findings are also consistent with a reduced phosphate burst. F-S1 was shown previously to have a reduced phosphate burst and the perturbation of the predominant intermediate from M** (*72*).

Skeletal and cardiac myosin transient intermediate concentrations are identical to within experimental error during steady-state ATPase in the native and TNP-modified forms. When SH1 is modified, both myosins have accelerated ATPases and M* as the predominant intermediate, but the second most populated intermediate is M^ in skeletal and M** in cardiac S1. This significant inconsistency is possibly the effect of differing local interactions between probe and protein in the two myosins. The local environment for fluorescein bound to S1 and βS1 differs detectable as is readily seen from their fluorescein CD spectra in Figure 9B. We know probe size and/or shape affects ATPase activation following SH1 modification in skeletal S1, probably because different probes interact differently with the protein (*30*), so it would follow that the same probe in the slightly altered binding sites of the two proteins might differently activate ATPase. While both proteins show ATPase activation with SH1 modification, how the probe destabilizes M** differs significantly in the two proteins.

DISCUSSION

In the heart muscle, cardiac myosin forms thick filaments with the S1 moieties, or cross-bridges, projecting outward away from the filaments. The S1's interact with actin filaments in the highly ordered lattice of the muscle sarcomere. Actomyosin interactions consume ATP while generating force to produce filament sliding. This process is the basis for muscle contraction. The kinetic scheme for myosin-catalyzed ATP hydrolysis with and without force generation, consists of the steps shown in Scheme 1. In the force producing step, the rotating cross-bridge model of contraction has the cross-bridge rotating after strong actin binding to develop torque and deliver the impulsive force to the actin filament (*73*, *74*). How S1 converts the free energy of ATP hydrolysis to work produced by filament sliding is the energy transduction mechanism.

ATP hydrolysis occurs in the ATP binding site within the S1 catalytic domain. From there, the effects of hydrolysis influence remote, spatially separate, sites including locations where actin binds and where torque is generated. The influences from hydrolysis propagate throughout S1 to the remote sites via pathways that when known will shape our models for energy transduction. Limited proteolysis, interrupting the S1 peptide backbone at surface loops while otherwise leaving the S1 intact, identifies potential functional subunits within S1 (*10*, *11*, *14*, *50*, *75*). Backbone cuts also identify energy transduction pathways if they decouple the active site from the remote sites normally under active site control. In skeletal S1, two surface loops (1 and 2) were identified and shown to be involved in the regulation of actin activated ATPase (loop 1) and actin binding (loop 2) (*13*, *58*, *76*−*79*). In cardiac S1, we showed that an additional surface loop (C-loop) is cleaved during limited proteolysis. Unlike skeletal S1, ATPase rates are dramatically affected by the cleavage of loop 1 and the C-loop placing these linkages within the energy transduction pathway. The rate of C-loop cleavage is accelerated by nucleotide binding to the active site of S1 again indicating energy transduction uses the C-loop for a pathway. The observed acceleration of steady-state Mg^{2+}-ATPase upon cleavage of loop 1 indicates the rate-limiting step in ATP hydrolysis, phosphate release, is likewise accelerated. The deceleration of the steady-state Mg^{2+}-ATPase upon cleavage of the C-loop cannot be as readily interpreted but its effect on ATPase transient intermediate fractional concentrations can in the future be addressed with the spectroscopic methods discussed subsequently.

The docking of skeletal S1 and F-actin involves loop 2 because bound actin is know to prevent proteolytic cleavage of loop 2 (*14*, *15*). The picture is changed for βS1 because actin allows cleavage of loop 2 (*8*) but inhibits cleavage of the C-loop. The C-loop is near to, but not within, a proposed actomyosin interface (*80*). These observations pertain to the site of actin binding but are open to many possible structural interpretations. They suggest it would be reasonable to view the actomyosin interface as dynamic and possibly serving as a site of torque generation (*81*) rather than as a simple static anchoring point for the transfer of momentum to the thin filament. Supporting this idea, multiple actoS1 conformations were reported to occur in muscle fibers in rigor (*82*) as were significant conformational change in the actomyosin interface during the weak to strong binding transition (*83*).

A site of torque generation *within* S1 has been proposed to reside in the converter region (*17*, *84*). There two conserved glycine residues, Gly697 and Gly708, are essential for function and suggested to be pivots in the peptide backbone facilitating lever arm movement (*85*, *86*). Consistent with this picture are certain spectroscopic signals originating from two interfaces of the catalytic, converter, and lever arm domains. Interface I contains SH1 and Trp508 (*22*, *52*, *53*, *87*). Interface II contains the reactive lysine residue (*45*). We have probed these critical regions of skeletal S1 and investigated their conformation during ATP hydrolysis and force generation. The result is a model for the cross-bridge cycle during contraction that details the successive structural changes in skeletal S1 that first hydrolyzes ATP then binds actin and produces force while releasing products (*29*, *30*). Herein we lay the groundwork for the identical characterization of the molecular mechanism of contraction for β-cardiac myosin.

Key to successful future work on the structural changes in βS1 during contraction is the use of nucleotide analogues. They induce static structures in skeletal S1 mimicking the Scheme 1 transients M*, M**, and M^ occurring during ATPase. Scheme 1 applies to βS1 (*3*−*5*), suggesting the nucleotide analogues may likewise induce structures in βS1 mimicking the transient intermediates. The investigation of

the nucleotide analogue effect on βS1 structure follows the pattern we established with skeletal S1. Previously, we found that the occupation of structural transient states during ATPase leaves a spectroscopic signature observable from S1+MgATP in the steady-state. By knowing the spectroscopic signature of each transient, the S1+MgATP signature is decomposed into the constituent states with weights equal to the fractional concentrations of the constituents. Assuming selected nucleotide analogues induced the desired constituent state structures, then using their observed spectroscopic signature to decompose the S1+MgATP signature, we arrived at the expected fractional concentration for the constituent transients establishing the one-to-one correspondence between analogue-induced and transient intermediate structure. This kind of spectroscopic decomposition of S1+MgATP was carried out using the near UV CD spectrum of the native skeletal S1 (*33*). Herein, we apply it to the same signal in βS1 and to signals originating from probes in interfaces I and II of modified βS1. Our findings establish the unique correspondence between the nucleotide analogue induced, and the real transient intermediate, structures in βS1. The work with probe signals permits investigation of the effect of probe modification on the kinetics of Scheme 1.

We investigated the nature of nucleotide analogue trapping of βS1 by studying trapping kinetics. Nucleotide analogue trapping of βS1 follows Scheme 4. Analogue association/dissociation occurs in two steps where rapidly reversible analogue binding precedes the slower isomerization and formation of the stable complex. Characteristic rates for these processes resemble those from skeletal S1 (Table 1). The actin-induced dissociation of the trap is likewise completed in two steps, one reversible, the other irreversible under the experimental conditions. The reversibly actin bound intermediate A···S1‡·ADP·PA remains to be structurally characterized. It possibly mimics a weakly actin bound cross-bridge in a muscle fiber except for its remarkable stability. Using the kinetic constants for the vanadate trap from Table 1, the weakly actin-bound transient reaches a steady-state fractional concentration of ~0.4 in the conditions for the actin-induced dissociation experiments. The irreversible decomposition of this state into the more stable A·S1 state takes place over hours.

Nucleotide binding to the active site of myosin perturbs the emission from the ATP-sensitive tryptophan signaling protein conformation change. In many myosin forms, including skeletal S1, the residue responsible for this response is Trp508 (*23*, *26*−*28*). We showed here by isolating Trp508 emission with differential spectroscopy that Trp508 in βS1 is an ATP-sensitive tryptophan and that its response to nucleotide or analogue binding or trapping is similar to that observed from Trp508 in skeletal S1 (*51*). Likewise reminiscent of skeletal S1 is the acrylamide quenching of Trp508. The quenching data shows that the conformation of interface I containing Trp508 changes in a stepwise fashion as the protein assumes the structure of the transient intermediates in Scheme 1. From the Trp508 intensity and quenching data, we estimated the fractional concentration of the Scheme 1 transient intermediates for βS1 (Table 3) obtaining results closely paralleling those from the near UV CD.

Coordinated interactions among myosin, actin, and nucleotide are manifest in the muscle machine. P_i release in M** is rate limiting and accelerated >100 fold upon actin binding ensuring coupling of ATP splitting and force generation (*3*, *88*). Alternatively, accelerated P_i release in M** increases the probability for ATP splitting without force generation. Thus, the P_i release rate is an efficiency modulator and a compelling target for efficiency degrading mutations. We have identified a candidate class of mutations implicated in HCM possibly affecting this type of defect. They reside in interfaces I and II where we have located spectroscopic probes that act as site-specific structural perturbants of βS1 mimicking mutations, and, as chiral reporter groups signaling the structural effect of modification. With these probes, we are ready to formulate and visualize a model for the cross-bridge cycle during contraction in the pattern set down for skeletal S1 (*29*, *30*).

Interface I contains the reactive thiol (Cys705), the ATP sensitive tryptophan (Trp508), and the Phe513Cys mutation implicated in HCM. Cys705 is located among the glycine swivels Gly697, Gly701, and Gly708. These swivels are essential for S1 function (*85*, *86*) and implicated in energy transduction (*84*). Structural characterization of this interface in skeletal S1 during contraction suggested the probes interfere with normal glycine swiveling to perturb the kinetics of Scheme 1 (*29*, *30*). We have shown here several consequences of fluorescein modification of SH1 in βS1 including its effect on ATPase kinetics (Table 4). The mechanism by which the ATPase kinetics are perturbed should implicate the responsible local interactions, as it did for skeletal S1, and suggest a role in similar effects for the Phe513Cys mutation.

Interface II contains Lys83, Arg721, and several mutations near Arg721 implicated in HCM (*9*, *19*). TNP modifying RLR has characteristic effects on the various ATPases of βS1 as shown here and elsewhere (*69*, *71*). Structural characterization of this interface in skeletal S1 during contraction suggested the mechanism for how the probe perturbs the ATPases (*29*, *30*). We found that lever arm movement in the M*·ATP → M**·ADP·P_i transition results in a lever arm/TNP collision. The collision interferes with formation and stability of the predominant M** intermediate accelerating P_i release. In the M, M*·ATP, and M^·ADP states Arg721, a residue residing on the lever arm side of interface II, interacts with the TNP at RLR. Mutation of a residue on the lever arm domain at or near Arg721 could create a lever arm/Lys83 collision leading again to predominant intermediate destabilization and acceleration of P_i release in the absence of actin.

CONCLUSIONS

We characterized tertiary structure and dynamics of βS1 with proteolytic digestion, appointment of the one-to-one correspondence between particular nucleotide analogue-induced structures and the transient states in the ATPase cycle, and with measurement of the nucleotide analogue trapping kinetics and fluorescence intensity and acrylamide quenching changes accompanying nucleotide or nucleotide analogue binding or trapping. Proteolytic digestion of βS1 splits the heavy chain at surface loops 1 and 2, and produces a new cut at Arg369 on the surface C-loop (Figure 1). The cleavage at loop 1 accelerates Mg^{2+}-ATPase ~2-fold, while cleavage at the C-loop returns the Mg^{2+}-ATPase to its level in native βS1, placing these linkages within the energy

Table 5: Products of Trypsin Proteolysis of βS1

species	amount	fragments in kDa
βS1	$f(-)$	95.6
βS1(1)	$f(1)$	25, 70.6
βS1(2)	$f(2)$	75.6, 20
βS1(1,2)	$f(1,2)$	25, 50.6, 20
βS1(1,C,2)	$f(1,C,2)$	25, 20.3, 30.3, 20
βS1(C)	$f(C)$	45.3, 50.3
βS1(1,C)	$f(1,C)$	25, 20.3, 50.3
βS1(C,2)	$f(C,2)$	45.3, 30.3, 20

transduction pathway. F-actin protects the C-loop but not loop 2 from proteolysis, suggesting that βS1 presents an actoβS1 conformation different from skeletal S1. Characterization of the βS1 structure following active site trapping with ADP·AlF_4^- shows that it most closely resembles the predominant ATPase intermediate M**·ADP·P_i from Scheme 1. By similar analysis, active site binding of ATPγS or ADP shows these analogues induce structures in βS1 most closely resembling the M*·ATP or M^·ADP intermediates from Scheme 1. The nucleotide analogue trapping kinetics were similar to those from skeletal S1 and revealed the presence of a reversible, weakly actin bound state for the M**·ADP·P_i analogues ADP·Vi and ADP·AlF_4^-. Trp508 fluorescence enhancement accompanies the binding or trapping of nucleotide or nucleotide analogue. Acrylamide quenching of Trp508 shows the conformation of interface I changes in a stepwise fashion as the protein assumes the structures of the transient intermediates in Scheme 1.

ACKNOWLEDGMENT

We thank Dr. Andras. Muhlrad (Hebrew University, Jerusalem, Israel) for helpful suggestions, Dr. György Hegyi (Eötvös Loránd University, Budapest, Hungary) for the muscle acetone powder used as the source of actin in all of our experiments, and Dr. Whyte Owen of Mayo Clinic for the molecular weight standards.

APPENDIX

Time-Resolved Proteolysis. Trypsin cuts the peptide backbone of myosin heavy chain at the surface loops. The βS1 heavy chain contains three such loops referred to as loops 1, 2, and C-loop in Scheme 2. These cuts occur in solution with certain kinetics such that, for given digestion conditions, various amounts of βS1 and its split forms are present. Table 5 lists the possible forms of βS1, where 1, C, and 2 in parentheses refer to the presence of the cut (see also Scheme 3). Fragments do not include the light chain that is present but ignored in all subsequent analysis.

The species βS1(C) and βS1(C,2) are eliminated from consideration because a peptide fragment with molecular mass of 45.3 kDa was never observed in the digest. The βS1-(1,C) species produces a 50.3-kDa fragment containing SH1. 5′-IAF specifically modifies SH1 in βS1 giving F-βS1. Digested F-βS1 produced proteolytic fragments such as those of βS1 but failed to produce a fluorescent 50.3-kDa fragment (Figure 3, lanes 9−10) ruling out the presence of the F-βS1-(1,C) species. Consequently, the possible species under consideration exclude the last three entries in Table 5.

We next establish relationships between Coomassie stained bands in the SDS−PAGE and the amount of the species in solution given by f. In the gel, some peptide fragments comigrate. We observed bands corresponding to the peptides with masses (in kDa): 95, 75.6+70.6, 50.6, 30.3, 25, and 20+20.3. The 75.6-kDa and 70.6-kDa peptides were separated and their relative contributions were estimated by performing an additional SDS−PAGE analysis of the samples on a 7% acrylamide gel. The 20- and 20.3-kDa peptides are indistinguishable. Gels analyzing the contents of digested βS1 as a function of time were scanned (Scanjet 4C, Hewlet Packard, Palo Alto, CA; image analysis with NIH Image) and amount of peptide in the bands estimated using the assumptions that (i) the total absorption for βS1 is conserved before and after digestion and (ii) the integrated absorption from a band is proportional to the (moles) × (length) of the peptide. Assumption (ii) follows from (i). Assumption (i) was verified by computing the total absorption from the bands in the gel originating from the heavy chain of βS1. Let g denote the amount of peptide in the band with a subscript identifying the approximate weight of the peptide, i.e., g_{95}, g_{75}, g_{70}, g_{50}, g_{30}, g_{25}, and g_{20}. The relationship between f and g expressed in matrix form,

$$\begin{pmatrix} 1 & 0 & 0 & 0 & 0 \\ 0 & 1 & 0 & 0 & 0 \\ 0 & 0 & 1 & 0 & 0 \\ 0 & 0 & 0 & 1 & 0 \\ 0 & 0 & 0 & 0 & 1 \\ 0 & 1 & 0 & 1 & 1 \\ 0 & 0 & 1 & 1 & 2 \end{pmatrix} \begin{pmatrix} f(-) \\ f(1) \\ f(2) \\ f(1,2) \\ f(1,C,2) \end{pmatrix} = \frac{1}{g_{95} + g_{75} + g_{70} + g_{50} + g_{30}} \begin{pmatrix} g_{95} \\ g_{70} \\ g_{75} \\ g_{50} \\ g_{30} \\ g_{25} \\ g_{20} \end{pmatrix} \quad (1A)$$

has the $1/(g_{95} + g_{75} + g_{70} + g_{50} + g_{30})$ prefactor to ensure the f's are fractional concentrations that sum to 1. In the initial stages of the mildest proteolytic digestion conditions, g_{25} and g_{20} were not quantitative because the longer peptide from the loop 2 cut (βL20k in Scheme 3) produced a diffuse band that migrated too closely to the β25k peptide. In this condition, the appropriate rows in the matrix in eq 1A were deleted. Equation 1A is solved at each observation time point by linear least squares with inequality constraints requiring the fractional concentrations to be ≥ 0.

REFERENCES

1. Jaenicke, T., Diederich, K. W., Haas, W., Schleich, J., Lichter, P., Pfordt, M., Bach, A., and Vosberg, H. P. (1990) *Genomics 8*, 194−206.
2. Morales, M. F., and Botts, J. (1979) *Proc. Natl. Acad. Sci. U.S.A. 76*, 3857−3859.
3. Marston, S. B., and Taylor, E. W. (1980) *J. Mol. Biol. 139*, 573−600.
4. Taylor, R. S., and Weeds, A. G. (1976) *Biochem. J. 159*, 301−315.
5. Smith, S. J., and Cusanovich, M. A. (1984) *J. Biol. Chem. 259*, 9365−9368.
6. Klotz, C., Leger, J. J., and Marotte, F. (1976) *Eur. J. Biochem. 65*, 607−611.

7. Muhlrad, A., Srivastava, S., Hollosi, G., and Wikman-Coffelt, J. (1981) *Arch. Biochem. Biophys. 209*, 304−313.
8. Applegate, D., Azarcon, A., and Reisler, E. (1984) *Biochemistry 23*, 6626−6630.
9. Rayment, I., Holden, H. M., Sellers, J. R., Fananapazir, L., and Epstein, N. D. (1995) *Proc. Natl. Acad. Sci. U.S.A. 92*, 3864−3868.
10. Bálint, M., Wolf, I., Tarcsafalvi, A., Gergely, J., and Sréter, F. A. (1978) *Arch. Biochem. Biophys. 190*, 793−799.
11. Mornet, D., Ue, K., and Morales, M. F. (1984) *Proc. Natl. Acad. Sci. U.S.A. 81*, 736−739.
12. Spudich, J. A. (1994) *Nature 372*, 515−518.
13. Murphy, C. T., and Spudich, J. A. (2000) *J. Muscle Res. Cell Motil. 21*, 139−151.
14. Mornet, D., Pantel, P., Audemard, E., and Kassab, R. (1979) *Biochem. Biophys. Res. Commun. 89*, 925−932.
15. Yamamoto, K., and Sekine, T. (1979) *J. Biochem. 86*, 1869−1881.
16. Rayment, I., Rypniewski, W. R., Schmidt-Base, K., Smith, R., Tomchick, D. R., Benning, M. M., Winkelmann, D. A., Wesenberg, G., and Holden, H. M. (1993) *Science 261*, 50−58.
17. Dominguez, R., Freyzon, Y., Trybus, K. M., and Cohen, C. (1998) *Cell 94*, 559−571.
18. Houdusse, A., Kalabokis, V. N., Himmel, D., Szent-Gyorgyi, A. G., and Cohen, C. (1999) *Cell 97*, 459−470.
19. Roberts, R., Marian, A. J., and Bachinski, L. (1998) *J. Cardiac Failure 2*, S87−S95.
20. Redwood, C. S., Moolman-Smook, J. C., and Watkins, H. (1999) *Cardiovasc. Res. 44*, 20−36.
21. Vikstrom, K. L., and Leinwand, L. A. (1996) *Curr. Opin. Cell Biol. 8*, 97−105.
22. Park, S., Ajtai, K., and Burghardt, T. P. (1996) *Biochim. Biophys. Acta 1296*, 1−4.
23. Park, S., and Burghardt, T. P. (2000) *Biochemistry 39*, 11732−11741.
24. Papp, S., and Highsmith, S. (1993) *Biochim. Biophys. Acta 1202*, 169−172.
25. Hiratsuka, T. (1992) *J. Biol. Chem. 267*, 14949−14954.
26. Batra, R., and Manstein, D. J. (1999) *J. Biol. Chem. 380*, 1017−1023.
27. Yengo, C. M., Chrin, L. R., Rovner, A. S., and Berger, C. L. (2000) *J. Biol. Chem. 275*, 25481−25487.
28. Onishi, H., Konishi, K., Fujiwara, K., Hayakawa, K., Tanokura, M., Martinez, H. M., and Morales, M. F. (2000) *Proc. Natl. Acad. Sci. U.S.A. 97*, 11203−11208.
29. Burghardt, T. P., Cruz-Walker, A. R., Park, S., and Ajtai, K. (2001) *Biochemistry 40*, 4821−4833.
30. Burghardt, T. P., Park, S., and Ajtai, K. (2001) *Biochemistry 40*, 4834−4843.
31. Fisher, A. J., Smith, C. A., Thoden, J. B., Smith, R., Sutoh, K., Holden, H. M., and Rayment, I. (1995) *Biochemistry 34*, 8960−8972.
32. Smith, C. A., and Rayment, I. (1996) *Biochemistry 35*, 5404−5417.
33. Peyser, Y. M., Ajtai, K., Werber, M. M., Burghardt, T. P., and Muhlrad, A. (1997) *Biochemistry 36*, 5170−5178.
34. Peyser, Y. M., Ajtai, K., Burghardt, T. P., and Muhlrad, A. (2001) *Biophys. J. 81*, 1101−1114.
35. Xing, J., and Cheung, H. C. (1994) *Arch. Biochem. Biophys. 313*, 229−234.
36. Brenner, B., Schoenberg, M., Chalovich, J. M., Greene, L. E., and Eisenberg, E. (1982) *Proc. Natl. Acad. Sci. U.S.A. 79*, 7277−7291.
37. Millar, N. C., and Geeves, M. A. (1988) *Biochem. J. 249*, 735−743.
38. Tonomura, Y., Appel, P., and Morales, M. (1966) *Biochemistry 5*, 515−521.
39. Weeds, A. G., and Taylor, R. S. (1975) *Nature 257*, 54−56.
40. Laemmli, U. K. (1970) *Nature 227*, 680−685.
41. Tada, M., Bailin, G., Bárány, K., and Bárány, M. (1969) *Biochemistry 8*, 4842−4850.
42. Pardee, J. D., and Spudich, J. A. (1982) *Methods Enzymol. 85*, 164−179.
43. Fiske, C. H., and Subbarow, Y. (1925) *J. Biol. Chem. 66*, 375−400.
44. Tashima, Y. (1975) *Anal. Biochem. 69*, 410−414.
45. Ajtai, K., Peyser, Y. M., Park, S., Burghardt, T. P., and Muhlrad, A. (1999) *Biochemistry 38*, 6428−6440.
46. Okuyama, T., and Satake, K. (1960) *J. Biochem. 47*, 454−462.
47. Mornet, D., Pantel, P., Bertrand, R., Audemard, E., and Kassab, R. (1980) *FEBS Lett. 117*, 183−188.
48. Ajtai, K., and Burghardt, T. P. (1992) *Biochemistry 31*, 4275−4288.
49. Bálint, M., Sréter, F. A., Wolf, I., Nagy, B., and Gergely, J. (1975) *J. Biol. Chem. 250*, 6168−6177.
50. Muhlrad, A., and Hozumi, T. (1982) *Proc. Natl. Acad. Sci. U.S.A. 79*, 958−952.
51. Werber, M. M., Peyser, Y. M., and Muhlrad, A. (1992) *Biochemistry 31*, 7190−7197.
52. Park, S., Ajtai, K., and Burghardt, T. P. (1996) *Biophys. Chem. 63*, 67−80.
53. Park, S., Ajtai, K., and Burghardt, T. P. (1997) *Biochemistry 36*, 3368−3372.
54. Trentham, D. R., Eccleston, J. F., and Bagshaw, C. R. (1976) *Q. Rev. Biophys. 9*, 217−281.
55. Maruta, S., Henry, G. D., Sykes, B. D., and Ikebe, M. (1993) *J. Biol. Chem. 268*, 7093−7100.
56. Goody, R. S., and Hofmann, W. (1980) *J. Muscle Res. Cell Motil. 1*, 101−115.
57. Adelstein, R. S., and Sellers, J. R. (1996) in *Biochemistry of Smooth Muscle Contraction* (Barany, M., Ed.) pp 8−12, Academic Press, New York.
58. Mornet, D., Pantel, P., Audemard, E., Derancourt, J., and Kassab, R. (1985) *J. Mol. Biol. 183*, 479−489.
59. Mocz, G., Szilagyi, L., Chen Lu, R., Fabian, F., Balint, M., and Gergely, J. (1984) *Eur. J. Biochem. 145*, 221−229.
60. Ajtai, K., Szilagyi, L., and Biro, E. N. A. (1982) *FEBS Lett. 141*, 74−77.
61. Hozumi, T., and Muhlrad, A. (1981) *Biochemistry 20*, 2945−2950.
62. Goodno, C. C. (1979) *Proc. Natl. Acad. Sci. U.S.A. 76*, 2620−2624.
63. Phan, B., and Reisler, E. (1992) *Biochemistry 31*, 4787−4793.
64. Goodno, C. C. (1982) *Methods Enzymol. 185*, 116−123.
65. Greene, L. E., and Eisenberg, E. (1980) *J. Biol. Chem. 255*, 543−548.
66. Highsmith, S. (1976) *J. Biol. Chem. 251*, 6170−6172.
67. Goodno, C. C., and Taylor, E. W. (1982) *Proc. Natl. Acad. Sci. U.S.A. 79*, 21−25.
68. Xu, S., Malinchik, S., Gilroy, D., Kraft, Th., Brenner, B., and Yu, L. C. (1997) *Biophys. J. 73*, 2292−2303.
69. Miyanishi, T., Inoue, A., and Tonomura, Y. (1979) *J. Biochem. 85*, 747−753.
70. Muhlrad, A. (1977) *Biochim. Biophys. Acta 493*, 154−166.
71. Muhlrad, A. (1983) *Biochemistry 22*, 3653−3660.
72. Sleep, J. A., Trybus, K. M., Johnson, K. A., and Taylor, E. W. (1981) *J. Muscle Res. Cell Motil. 2*, 373−399.
73. Huxley, H. E. (1969) *Science 164*, 1356−1366.
74. Huxley, A. F., and Simmons, R. M. (1971) *Nature 233*, 533−538.
75. Szilágyi, L., Bálint, M., Sréter, F. A., and Gergely, J. (1979) *Biochem. Biophys. Res. Commun. 87*, 936−945.
76. Knetsch, M. L. W., Uyeda, T. Q. P., and Manstein, D. J. (1999) *J. Biol. Chem. 274*, 20133−20138.
77. Murhpy, C. T., and Spudich, J. A. (1999) *Biochemistry 38*, 3785−3792.
78. Bobkov, A. A., Bobkova, E. A., Lin, S. H., and Reisler, E. (1996) *Proc. Natl. Acad. Sci. U.S.A. 93*, 2285−2289.
79. Joel, P. B., Trybus, K. M., and Sweeney, H. L. (2001) *J. Biol. Chem. 276*, 2998−3003.
80. Mendelson, R. A., and Morris, E. P. (1997) *Proc. Natl. Acad. Sci. U.S.A. 94*, 8533−8538.
81. Nihei, T., Mendelson, R. A., and Botts, J. (1974) *Proc. Natl. Acad. Sci. U.S.A. 71*, 274−277.
82. Andreev, O. A., Takashi, R., and Borejdo, J. (1995) *J. Muscle Res. Cell Motil. 16*, 353−367.

83. Xu, J., and Root, D. D. (2000) *Biophys. J. 79*, 1498−1510.
84. Geeves, M. A., and Holmes, K. C. (1999) *Annu. Rev. Biochem. 68*, 687−728.
85. Kinose, F., Wang, S. X., Kidambi, U. S., Moncman, C. L., and Winkelmann, D. A. (1996) *J. Cell Biol. 134*, 895−909.
86. Patterson, B., Ruppel, K. M., Wu, Y., and Spudich, J. A. (1997) *J. Biol. Chem. 272*, 27612−27617.
87. Burghardt, T. P., Garamszegi, S. P., Park, S., and Ajtai, K. (1998) *Biochemistry 37*, 8035−8047.
88. Sellers, J. R., and Goodson, H. V. (1995) *Protein Profile 2*, 1323−1423.
89. Ratkowsky, D. A. (1983) in *Nonlinear Regression Modeling: A Unified Approach*; pp 13−47, Marcel Dekker, Inc, New York.
90. Sweeney, H. L., Straceski, A. J., Leinwand, L. A., Tikunov, B. A., and Faust, L. (1994) *J. Biol. Chem. 269*, 1603−1605.

BI0112098